CME LIVE OPEN ACCESS

Electrical Electronics Engineering: Open Access

Research Article

Design and Simulation-Based Verification of an 1100-kV AC Grid Substation Supplying a 10-GW Load

Mohammad Ali*

School of Science and Engineering, Atlantic International University, Honolulu, HI 96813 USA

Corresponding Author: Mohammad Ali, School of Science and Engineering, Atlantic International University, Honolulu, HI 96813 USA .

Received: 2026 Sep 28 **Accepted:** 2026 Oct 30 **Published:** 2026 Nov 06

Abstract

This paper presents the design of an ultra-high-voltage (UHV) ac substation with a highest voltage for equipment of 1100 kV that delivers 10 GW into a 400-kV network and verifies every rating-determining decision by simulation. Four 1100-kV feeders (2 × 280 km and 2 × 320 km, 8 × ACSR 630/45, surge-impedance loading 4203 MW) supply five banks of 3 × 1000-MVA single-phase autotransformers, and twelve 420-kV feeders on six double-circuit routes distribute it. One consistent set of models supports the design: Carson–Deri line parameters, a 24-bus Newton–Raphson load flow with N-1, N-2 and P–V analysis, IEC 60909 sequence-network short-circuit analysis, multimachine transient stability, a three-phase Bergeron electromagnetic-transient model with Monte Carlo switching, IEC 60287 and IEC 60076-7 thermal models, and a two-layer boundary-element grounding model. Simulation revealed six findings missed by a deterministic preliminary design: with solidly grounded neutrals the single-phase fault at a two-bank 420-kV section reaches the full 63-kA rating, which a 10-Ω neutral reactor reduces to 48.4 kA; 1600 Mvar of switched capacitors is needed to keep the STATCOMs in reserve; a stuck center breaker gives a critical clearing time of 108 ms, shorter than the 150-ms breaker-failure clearing, which 1.1-GW generation rejection raises to 166 ms; transformer-terminal and bay-located gas-insulated arresters are indispensable; the 420-kV transformer connections require gas-insulated lines in hot desert soil; and autotransformer neutral-current reversal makes the grid discharge 69.8 kA, more than the fault current. The verified design has 1800/2400-kV switching/lightning withstand levels with 3.7–8.5% and 15.5% margins, a 55% voltage-stability margin and 99.83% full-load efficiency.

Keywords: Autotransformers, Electromagnetic transients, Gas-insulated transmission lines, Grounding, Insulation coordination, Power system stability, Short-circuit currents, Substation design, Ultra-high-voltage (UHV) transmission

1. Introduction

Ultra-high-voltage (UHV) ac transmission, with nominal voltages of 1000 kV and above, carries several gigawatts per circuit over distances of a few hundred kilometers and is the backbone technology for connecting remote generation hubs to load centers [1,2]. Since the first 1000-kV demonstration project entered commercial operation in China in 2009, UHV ac substations with highest voltages for equipment of 1100 kV have been built in increasing numbers, and international guidance has followed in the form of CIGRE technical brochures and the IEC TS 63042 series [3-6]. Although IEC 60071-1 and IEC 62271-100 now list 1100-kV values, many application rules, test conditions and apparatus ratings in the mainstream standards are still established for systems up to 800 kV, so the designer of an 1100-kV substation must derive many ratings from first principles.

Substation design studies are usually deterministic: transformer loading is assessed by equal sharing, fault levels by the three-phase value, overvoltages by assumed representative values, and cable ratings by standard installation conditions. At UHV these simplifications are risky because the margins are thin. The breaker is rated at 63 kA with no higher standard value, the insulation levels are a compromise between withstand and apparatus size, and the transfer through a single busbar is large enough for a slow fault clearance to threaten the stability of entire generation hubs. Published work treats the individual problems insulation coordination with electromagnetic-transient (EMT) studies gas-insulated transmission lines (GIL) secondary-arc suppression grounding in layered soil but integrated designs that carry one data set through every study and report the margins actually achieved are rare [7-15].

This paper presents such an integrated design for a substation that receives 10 GW over four 1100-kV feeders and delivers it through twelve 420-kV feeders, at a hot desert site (50 °C) where the thermal conditions are more onerous than those on which most UHV experience is based. The contributions are:

• A design-by-simulation workflow in which line parameters, load flow, short circuit, stability, EMT, thermal behavior, cable rating and grounding are computed from one consistent data set (Figure 1);
• The identification of the single-phase fault as the governing short-circuit duty at a 420-kV section fed by two delta-tertiary autotransformers, and its mitigation by a neutral reactor;
• A reactive-power plan, quantified by load flow, that keeps the STATCOMs as a dynamic reserve despite fixed UHV line reactors and 18% transformer impedance;
• Statistical switching and fast-front lightning simulation that establishes the margins behind the 1800-kV and 2400-kV withstand levels and the necessity of transformer-terminal and bay-located gas-insulated arresters;
• A breaker-failure stability finding and its resolution by generation rejection;
• Thermal verification of GIL, cables and transformers at 50 °C, and a boundary-element grounding analysis that captures the neutral-current reversal of autotransformers.
• Section II defines the design basis and the feeder plan, and Section III states the mathematical models. Sections IV–XV present the feeder design, the configuration, and the system, transient, thermal, grounding, protection and economic studies. Section XVI compares the simulation-verified design with deterministic practice, and Section XVII concludes.

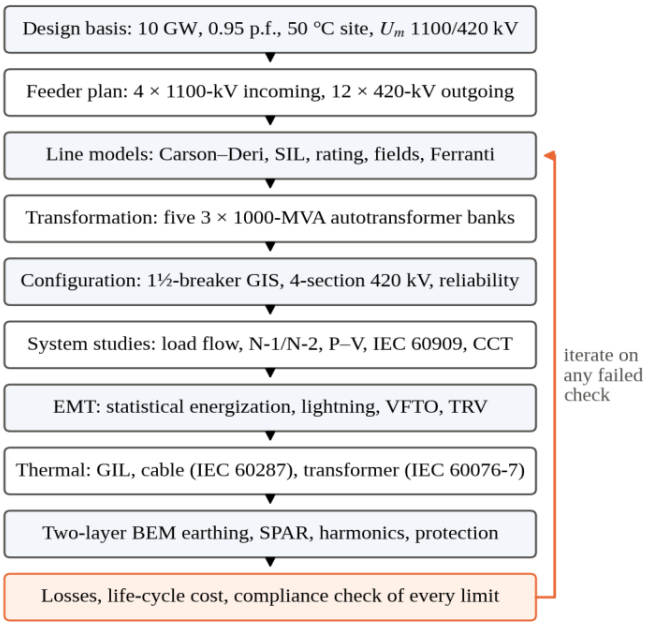


Figure 1: Design-by-Simulation Workflow. Every Result is Compared with A Limit Taken from a Standard; a Failed Check Returns the Design to the Decision that Caused it

2. Design Basis and Feeder Planning

2.1. Load and Site

The voltages follow IEC 60038 under which 1100 kV is the highest voltage for equipment of a 1000-kV nominal system [16]. The delivered power of 10,000 MW is converted to apparent power at an assumed power factor of 0.95 at the 420-kV busbars, and a planning margin of 10% is added because the transformation capacity of a UHV substation cannot easily be augmented once the switchyard is built:

$$S = P/\cos\varphi = 10{,}526 \text{ MVA}$$

$$S_{\mathrm{d}} = 1.1\,S = 11{,}580 \text{ MVA}. \quad (1)$$

The corresponding design currents are $I_{\mathrm{UHV}} = S_{\mathrm{d}}/\left(\sqrt{3}\,U_n\right)$ =6686 A at 1000 kV and 16,714 A at 400 kV. The site is an inland desert location at 500-m altitude; its conditions (Table 1) are used consistently in every thermal, insulation and grounding calculation.

Parameter	Value
Nominal / highest voltage	1000/1100 kV; 400/420 kV; tertiary 63/72.5 kV
Delivered power; power factor	10,000 MW; 0.95 lagging
Air temperature	50 °C max.; 35–50 °C design day; 28 °C yearly mean
Altitude; relative air density	500 m; δ = 0.853 at 50 °C
Solar radiation; wind (rating)	1000 W/m^2; 0.6 m/s
Ground temperature; soil thermal resistivity	30 °C at 1.5 m; 1.5 K•m/W (backfill 0.8)
Soil electrical resistivity	100 Ω•m to 20 m, 250 Ω•m below
Pollution class	c (medium), seasonal dust
Frequency; neutral treatment	50 Hz; effectively grounded

Table 1: Design Basis and Site Conditions

2.2. Number of Incoming Feeders

Each 1100-kV feeder is an eight-conductor single circuit with a surge-impedance loading (SIL) of 4203 MW (Section 4). For lines of 280–320 km the practical post-contingency limit is set by voltage regulation and angular stability rather than by the thermal rating, and is taken for planning as 1.2 SIL. The N-1 criterion then requires

$$n_{\text{in}} \geq \frac{P_{\text{imp}}}{1.2\,\text{SIL}} + 1 = \frac{10{,}010}{1.2 \times 4203} + 1 = 2.98. \quad (2)$$

Three feeders would satisfy (2) only at its limit and only if the power of a lost circuit could be shared evenly, which a two-corridor structure does not allow. Four feeders in two independent double-circuit corridors are therefore adopted (Table 2): L1 and L2 from generation hub A (280 km) and L3 and L4 from hub B (320 km). A fifth line position is reserved.

Feeder	Source, length	Peak flow received	N-1 maximum
L1, L2	Hub A, 280 km	2520 MW, 1499 A	5044 MW, 3005 A
L3, L4	Hub B, 320 km	2483 MW, 1473 A	4936 MW, 2945 A
L5	Reserved	–	–

Table 2: Incoming 1100-kv Feeder Schedule

2.3. Number of Outgoing Feeders

The outgoing feeders are quad ACSR "Moose" circuits of 60–120 km with a SIL of 678 MW and a thermal capability of 3326 A at 50 °C. With a loading factor $k_{\text{SIL}} \approx 1.3$, appropriate to circuits of this length,

$$n_{\text{out}} \geq \frac{P}{k_{\text{SIL}}\,\text{SIL}_{400}} = \frac{10{,}000}{1.3 \times 678} = 11.3 \rightarrow 12. \quad (3)$$

Twelve circuits on six double-circuit routes give an average of 833 MW (1.23 SIL) per circuit. The two circuits of each route terminate on different 420-kV sections, so that a section outage never removes a whole route. The assignment of circuits to sections (Table 3) was obtained by a local search that minimized the spread of bank loadings in the load flow; it narrowed the spread from 63–75% for an intuitive assignment to 66.1–69.7%.

Route	Length	Sections (a/b)	Peak flow a/b (MW)	Worst N-1 current
R1	60 km	S4/S2	1049/1081	2223 A
R2	80 km	S2/S1	885/857	1983 A
R3	100 km	S1/S3	724/698	1339 A
R4	70 km	S1/S4	952/957	2031 A
R5	90 km	S1/S3	797/767	1432 A
R6	120 km	S1/S3	627/606	1191 A

Table 3: Outgoing 420-Kv Feeder Schedule

2.4. Transformation Capacity

The largest standard UHV transformer unit is the 1000-MVA single-phase autotransformer, whose size is set by transport limits. One bank of three units is rated 3000 MVA, so that

$$n_b = \left\lceil \frac{S_d}{S_{bank}} \right\rceil + 1 = \left\lceil \frac{11{,}580}{3000} \right\rceil + 1 = 5 \quad (4)$$

banks give 15,000 MVA installed and 12,000 MVA firm, with one spare single-phase unit on site that restores any bank within 72 h. The banks are YNa0d11 autotransformers rated 1050/√3 / 420/√3 / 63 kV with an HV–MV impedance of 18% on 1000 MVA, chosen high to limit the 420-kV fault level, and HV–tertiary and MV–tertiary impedances of 62% and 40% on 334 MVA. The on-load tap changer has ±8 steps of 1.25% at the neutral end of the common winding. Because the site exceeds the 40 °C/30 °C/20 °C cooling-air limits of IEC 60076-2 the temperature-rise limits are reduced by 10 K to 50 K (top oil), 55 K (average winding) and 68 K (hot spot) [17].

The network model two generation-hub equivalents of 7300 and 6700 MVA, six load-center buses LC1–LC6 with a 400-kV tie ring, and a regional-grid equivalent EXT with 5000 MW of local generation—has 24 buses (Figure 2); its data are given in the Appendix.

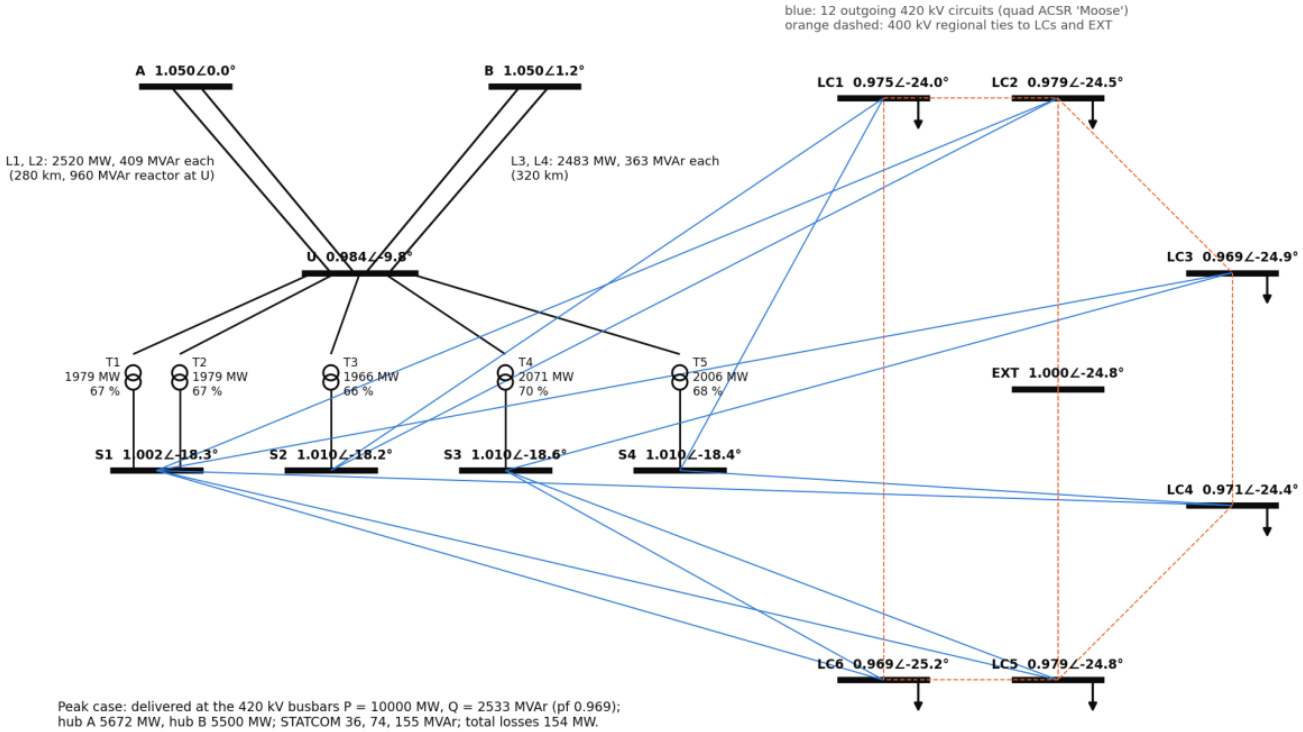


Figure 2: Network Model with the Peak Load-Flow Solution: Bus Voltages (Magnitude and Angle), UHV Feeder Flows and Bank Loadings. Blue: The Twelve Outgoing 420-kV Feeders; Dashed: Regional 400-kV Ties

3. Mathematical Models

All models were written for this work in Python (NumPy/SciPy) and share one data set. Network studies use a 1000-MVA base with voltage bases of 1000, 400 and 63 kV, so that the autotransformer ratio 1050/420 kV is unity in per unit; overvoltages are expressed in per unit of the peak phase-to-ground value of U_m, 1 p.u. = 898 kV. The equivalent circuits are shown in Figure 3 and the EMT circuits in Figure 4.

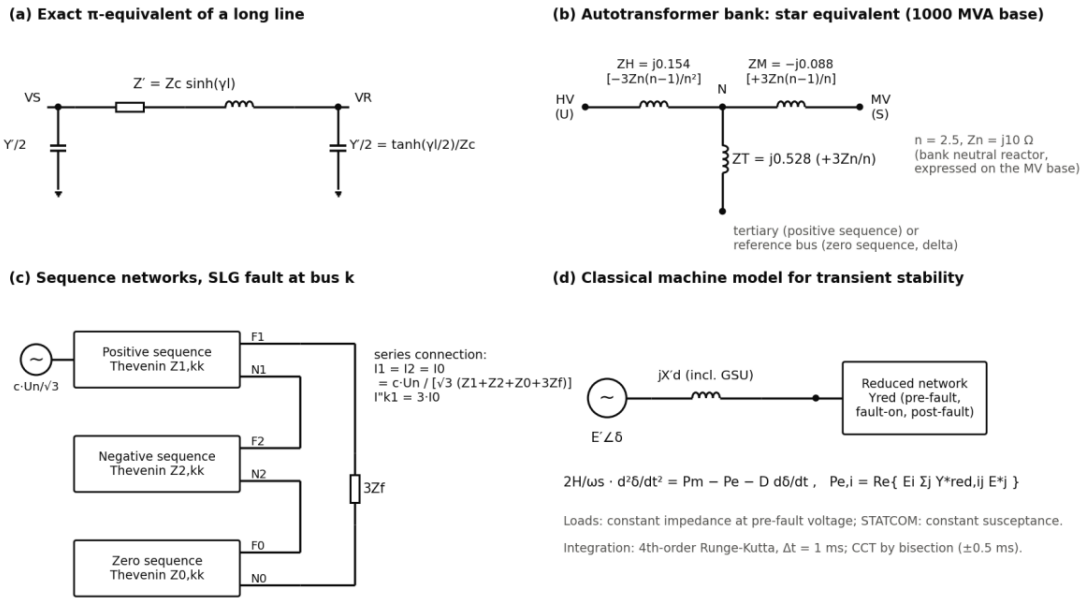


Figure 3: Equivalent Circuits Used in the System Studies: (a) Exact Π-Equivalent of a Long Line (b) Star Equivalent of an Autotransformer Bank with Neutral Reactor (c) Sequence-Network Connection for a Single-Phase-To-Ground Fault (d) Classical Machine Model

3.1. Transmission-Line Parameters

For conductors above an earth of resistivity ρ, the series impedances follow Carson's theory in the complex-depth form of Deri et al. [18,19].

$$p = \sqrt{\rho/(j\omega\mu_0)}$$

$$Z_{ii} = R_i + j\frac{\omega\mu_0}{2\pi}\ln\frac{2(h_i+p)}{\mathrm{GMR}_i} \tag{5}$$

$$Z_{ij} = j\frac{\omega\mu_0}{2\pi}\ln\frac{\sqrt{(x_i-x_j)^2+(h_i+h_j+2p)^2}}{d_{ij}} \tag{6}$$

and the potential coefficients follow from the method of images,

$$P_{ii} = \frac{1}{2\pi\varepsilon_0}\ln\frac{2h_i}{r_{\mathrm{eq},i}}, \quad P_{ij} = \frac{1}{2\pi\varepsilon_0}\ln\frac{D'_{ij}}{d_{ij}}. \tag{7}$$

A bundle of n subconductors of radius r and geometric mean radius g on a circle of radius $R_b = s/[2\sin(\pi/n)]$ is replaced by an equivalent conductor with

$$\mathrm{GMR}_b = \sqrt[n]{n\,g\,R_b^{n-1}}, \qquad r_{\mathrm{eq}} = \sqrt[n]{n\,r\,R_b^{n-1}}. \tag{8}$$

Ground wires are eliminated by Kron reduction, $C = P^{-1}$, and for a transposed circuit with mean self and mutual impedances Z_s and Z_m the sequence impedances are $Z_1 = Z_s - Z_m$ and $Z_0 = Z_s + 2Z_m$. With $\gamma = \sqrt{zy}$ and $Z_c = \sqrt{z/y}$, the exact π-equivalent (Figure 3(a)) and the voltage at a distance x from the receiving end are

$$Z' = Z_c\sinh\gamma l, \qquad \frac{Y'}{2} = \frac{1}{Z_c}\tanh\frac{\gamma l}{2} \tag{9}$$

$$V(x) = V_R\cosh\gamma x + Z_c I_R\sinh\gamma x. \tag{10}$$

The conductor rating follows the heat balance of IEEE Std 738 and CIGRE TB 601 and the maximum surface gradient of a bundle carrying charge q is compared with Peek's visual corona-onset gradient here in kV/cm (rms) with r in cm, surface factor m and relative air density δ [20-22].

$$I = \sqrt{\frac{q_c + q_r - q_s}{R_{ac}(T_c)}} \tag{11}$$

$$E_{\max} = \frac{q}{2\pi\varepsilon_0 nr}\left[1 + \frac{(n-1)r}{R_b}\right]$$

$$E_0 = 21.2\,m\,\delta\left(1 + \frac{0.301}{\sqrt{\delta r}}\right) \tag{12}$$

3.2. Autotransformer Bank

A bank is represented by its star equivalent (Figure 3(b)), obtained from the pair impedances as Z_H =

$\frac{1}{2}(Z_{HM}+Z_{HT}-Z_{MT})$ and cyclically. Referred to the 1000-MVA base and multiplied by $(1050/1000)^2$, the 18%/62%/40% pair impedances give $z_H = j0.1541$, $z_M = -j0.0880$ and $z_T = j0.5281$ p.u. per bank. In the zero-sequence network the delta tertiary connects the star point to the reference through Z_T, and a neutral impedance Z_n (on the MV base, ratio $n = U_H/U_M$) modifies the branches as [23].

$$Z_{H0} = Z_H - 3Z_n\frac{n-1}{n^2}$$

$$Z_{M0} = Z_M + 3Z_n\frac{n-1}{n}$$

$$Z_{T0} = Z_T + \frac{3Z_n}{n} \tag{13}$$

The neutral current is $I_N = 3(I_{0H} + I_{0M})$, with both zero-sequence currents in amperes and taken as flowing into the bank; its sign reverses when the MV system is the stronger zero-sequence source, a property that governs the grounding design (Section 13).

3.3. Load Flow and Short Circuit

The load flow solves $\mathbf{S} = \mathbf{V}\circ\overline{\mathbf{YV}}$ by the Newton–Raphson method in polar coordinates [24].

$$\begin{bmatrix}\Delta\mathbf{P}\\ \Delta\mathbf{Q}\end{bmatrix} = \begin{bmatrix}\partial\mathbf{P}/\partial\boldsymbol{\theta} & \partial\mathbf{P}/\partial|\mathbf{V}|\\ \partial\mathbf{Q}/\partial\boldsymbol{\theta} & \partial\mathbf{Q}/\partial|\mathbf{V}|\end{bmatrix}\begin{bmatrix}\Delta\boldsymbol{\theta}\\ \Delta|\mathbf{V}|\end{bmatrix} \tag{14}$$

with an analytical Jacobian, reactive-limit switching of generator and STATCOM buses, a convergence tolerance of 10^{-8} p.u., and an outer loop that scales the load-center demands until the specified power is delivered at the 420-kV busbars. Contingencies are simulated by removing the element, applying any automatic post-contingency action and re-solving; P–V curves are traced in 2% load steps until the iteration diverges at the nose.

Short circuits follow IEC 60909-0 with sequence bus-impedance matrices assembled from series impedances only and the voltage factor $c = 1.1$:

$$I''_{k3} = \frac{cU_n}{\sqrt{3}\,|Z_1|}, \qquad I''_{k1} = \frac{\sqrt{3}\,cU_n}{|Z_1+Z_2+Z_0|} \tag{15}$$

$$i_p = \kappa\sqrt{2}\,I''_k, \quad \kappa = 1.02 + 0.98\,e^{-3R/X}$$

$$\tau = (X/R)/(2\pi f) \tag{16}$$

For ground faults the zero-sequence branch currents, $\mathbf{V}_0 = -\mathbf{Z}_0[:,k]\,I_0$, give the division of the fault current between local neutrals and remote sources [25].

3.4. Transient Stability

Each area is represented by a classical machine (Figure 3(d)), loads by constant admittances and STATCOMs by constant susceptances. The network is Kron-reduced to the internal nodes for the pre-fault, fault-on and post-fault configurations, and the swing equations

$$\frac{2H_i}{\omega_S}\frac{d^2\delta_i}{dt^2} = P_{m,i} - P_{e,i}$$

$$P_{e,i} = \mathrm{Re}\left\{E_i\sum_j \overline{Y_{\mathrm{red},ij}E_j}\right\} \tag{17}$$

are integrated by the fourth-order Runge–Kutta method with a 1-ms step [26]. Instability is declared when any two rotor angles separate by more than 180° within 3 s, and the critical clearing time (CCT) is found by bisection to 1 ms. Unsymmetrical faults are represented by the shunt $Z_2 + Z_0$ at the fault bus.

3.5. Electromagnetic Transients

Following Dommel inductances and capacitances are replaced by trapezoidal companion models, e.g. [27,28].

$$i_L(t) = \frac{\Delta t}{2L}v(t) + \left[i_L(t-\Delta t) + \frac{\Delta t}{2L}v(t-\Delta t)\right]. \tag{18}$$

A transposed line is decoupled into one ground and two aerial Clarke modes, each a Bergeron line of surge impedance Z_c and travel time τ with its resistance lumped at the ends and middle; with $Z = Z_c + R/4$ and $h = (Z_c - R/4)/Z$, the history current at end k is

$$I_k(t) = \frac{1+h}{2}\left[-\frac{v_m(t-\tau)}{Z} - h\,i_{mk}(t-\tau)\right]$$

$$+\frac{1-h}{2}\left[-\frac{v_k(t-\tau)}{Z} - h\,i_{km}(t-\tau)\right]. \tag{19}$$

Metal-oxide (MO) arresters use piecewise log-linear V–I characteristics solved by Newton iteration with compensation; breakers are time-varying conductances with optional pre-insertion resistors. The statistical study runs 200 closing operations per case with a uniformly distributed closing instant and Gaussian pole scatter (σ = 1 ms, truncated at ±3 ms), and evaluates the 2% value by the phase-peak method [29].

3.6. Thermal Models

The transformer top-oil temperature θ_o and hot-spot rise follow the differential equations of IEC 60076-7 [30-31] for a load factor $K(t)$ and ambient $\theta_a(t)$:

$$\left[\frac{1+K^2R}{1+R}\right]^x \Delta\theta_{or} = k_{11}\tau_o\frac{d\theta_o}{dt} + (\theta_o - \theta_a) \quad (20)$$

$$k_{21}K^y Hg_r = k_{22}\tau_w\frac{d\Delta\theta_{h1}}{dt} + \Delta\theta_{h1}$$

$$(k_{21}-1)K^y Hg_r = \frac{\tau_o}{k_{22}}\frac{d\Delta\theta_{h2}}{dt} + \Delta\theta_{h2} \quad (21)$$

with $\theta_h = \theta_o + \Delta\theta_{h1} - \Delta\theta_{h2}$ and the relative aging rate of thermally upgraded paper

$$V = \exp\left(\frac{15{,}000}{383} - \frac{15{,}000}{\theta_h + 273}\right), \qquad L = \int V\,dt. \quad (22)$$

The rating of an unarmored single-core cable follows IEC 60287 [32,33]

$$I = \sqrt{\frac{\Delta\theta - W_d(0.5T_1 + T_3 + T_4)}{R[T_1 + (1+\lambda_1)(T_3+T_4)]}}, \quad (23)$$

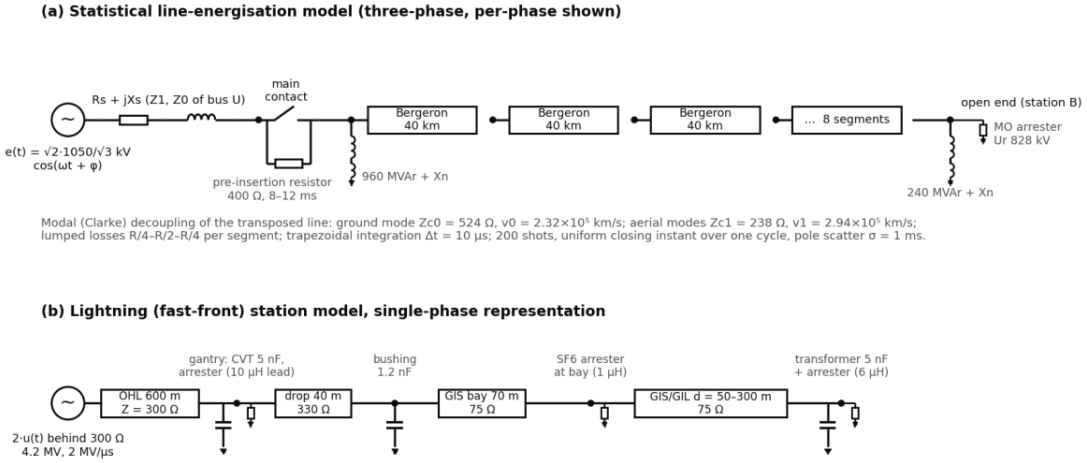


Figure 4: EMT Model Circuits: (a) Three-Phase Statistical Line-Energization Model; (b) Single-Phase Fast-Front Station Model

where T_4 of the hottest cable includes mutual heating and the backfill correction (Section X). The GIL conductor and enclosure temperatures are obtained from a two-node heat balance with natural convection in the pressurized gas (Kuehn–Goldstein) convection to air (Churchill–Chu) radiation and solar gain [34,35].

3.7. Grounding, Reliability and Economics

The grid and rods are divided into 6143 segments, each leaking a uniform current, and the two-layer soil is represented by the image series with reflection coefficient $K = (\rho_2 - \rho_1)/(\rho_2 + \rho_1)$ [13,14]:

$$G = \frac{\rho_1}{4\pi}\left\{\frac{1}{r_0} + \frac{1}{r'_0} + \sum_{n=1}^{N} K^n \sum_{q=1}^{4}\frac{1}{r_{nq}}\right\}. \quad (24)$$

Imposing a uniform grid potential yields the leakage currents, the grid resistance R_g and, by superposition, the surface potential. The reliability model enumerates active failures of breakers and busbars, stuck-breaker events, overlapping outages and maintenance states, and evaluates connectivity and curtailment over a six-step load–duration curve [36]. Present values use a 40-year life and an 8% discount rate:

$$\mathrm{PVF} = \frac{1-(1+r)^{-N}}{r} = \frac{1-1.08^{-40}}{0.08} = 11.92. \quad (25)$$

3.8. Verification of the Models

Each model was checked against an independent calculation before use. The line model gives C_1 = 14.30 nF/km and Z_c = 237.9 Ω, consistent with published 1000-kV values. The load flow closes the power balance to better than 10^{-6} MW. A single bank fed from an infinite 1100-kV source contributes $1.1\times400/(\sqrt{3}\times0.0662\times160)$=24.0 kA to a 420-kV fault, matching the short-circuit model. The EMT line reproduces the steady-state Ferranti rise of (10) to 0.04%, an undisturbed stability run drifts by less than 10^{-13} degrees in 10 s, and the transformer model reproduces the IEC 60076-7 steady-state rises of 45.0 K and 65.0 K exactly. The two-layer grid resistance lies between the uniform-soil values for ρ_1 and ρ_2, as it must.

4. Feeder Design

4.1.1100-kV Feeders

Each phase is an eight-conductor bundle of ACSR 630/45 (33.8 mm, 0.04633 Ω/km at 20 °C) with 400-mm

subconductor spacing, so that (8) gives R_b = 0.5226 m, GMR_b = 0.4298 m and r_{eq} =0.4414 m. The two circuits of a corridor share double-circuit towers with vertical phases at average heights of 74, 54 and 34 m, horizontal offsets of ±16, ±18 and ±17 m, and two OPGW ground wires at ±12 m, 92 m; the lowest mid-span clearance is 25 m. With an earth resistivity of 100 Ω•m, [5-7] and Kron reduction give the parameters of Table 4.

Quantity	Value
R_1 / X_1	0.00801 / 0.2543 Ω/km
R_0 / X_0	0.1314 / 0.7095 Ω/km
C_1 / C_0	14.30 / 8.22 nF/km
Zero-sequence mutual (between circuits)	0.123 + j0.368 Ω/km
Z_c, aerial / ground mode	237.9 / 524.3 Ω
Surge-impedance loading	4203 MW
Charging power at 1000 kV	4.49 Mvar/km
Thermal rating (90 °C, 50 °C ambient)	8 × 1011 = 8088 A
Max. surface gradient / onset gradient	15.4 / 18.6 kV/cm

Table 4: Parameters of the 1000-kV Feeders (per Circuit, 75 °C)

4.1.1. Thermal Rating: At 50 °C ambient, 0.6-m/s wind, 1000-W/m^2 sun and 500-m altitude, the heat-balance terms of (11) per meter are 57.8 W (convection), 31.2 W (radiation) and 27.0 W (solar), so that with R_{ac} = 0.0606 Ω/km at 90 °C a subconductor carries 1011 A and a phase 8088 A (14,010 MVA). The largest current in any N-1 case is 3005 A, 37% of this rating: the feeders are stability-limited, as long UHV lines normally are.

4.1.2. Corona and Fields: With every phase at $U_m/\sqrt{3}$, (12) gives maximum surface gradients of 13.6, 15.4 and 14.1 kV/cm (rms) on the top, middle and bottom phases, against an onset gradient of 18.6 kV/cm for a weathered conductor (m = 0.82) at the site air density δ = 0.853. The worst ratio, 0.83, meets the usual UHV target of about 0.85; the eight-conductor bundle is the smallest that does so. The ground-level electric field (Figure 5) peaks at 9.58 kV/m under the outer phases and falls below the 5-kV/m ICNIRP public reference level 35 m from the center line; the magnetic flux density does not exceed 15.8 μT [37].

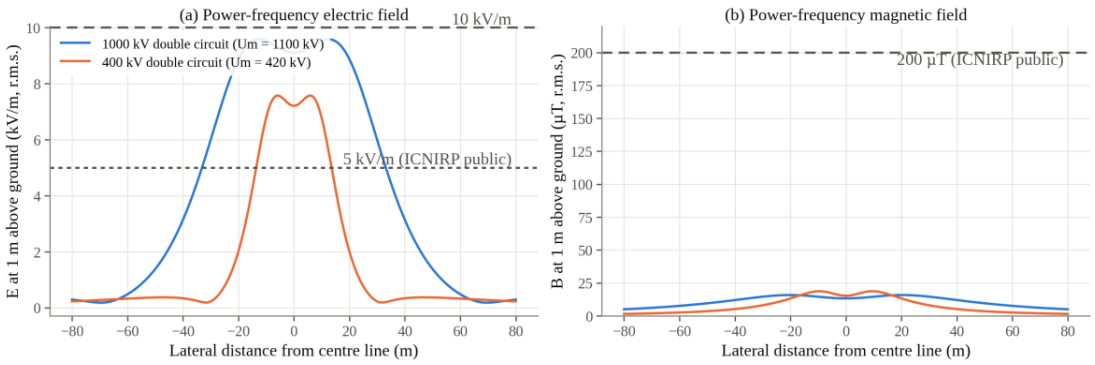


Figure 5: Ground-Level (1 m) Fields Under the 1000-kV and 400-kV Double-Circuit Feeders at U_m: (a) Electric Field; (b) Magnetic Flux Density

4.1.3. Ferranti Effect and Shunt Compensation: For the 320-km feeders the phase constant is βl = 0.342 rad, so an open line energized at 1.05 p.u. would reach 1.05/cosβl=1.115 p.u. at its open end, above U_m. With the 960-Mvar reactor (rated at 1050 kV; reactance X_r = 1148 Ω) at the substation end

$$V_R = \frac{V_S}{\cos\beta l + (Z_c/X_r)\sin\beta l}$$

$$= \frac{1.05}{0.942 + 0.207 \times 0.335} = 1.038 \qquad (26)$$

p.u., with a maximum of 1.060 p.u. along the line (Figure 6). Each feeder carries a 960-Mvar reactor (3 × 320 Mvar single-phase) at the substation and a 240-Mvar reactor at the remote end; with a total charging of 5390 Mvar for the four feeders, the degree of compensation is 86.6% for the 280-km and 75.8% for the 320-km lines. At the peak load (0.59 SIL) the voltage falls monotonically from 1.05 p.u. at the hub to 0.984 p.u. at the substation, because the fixed reactors absorb more than the lightly loaded line generates; this is the origin of the reactive deficit quantified in Section VI.

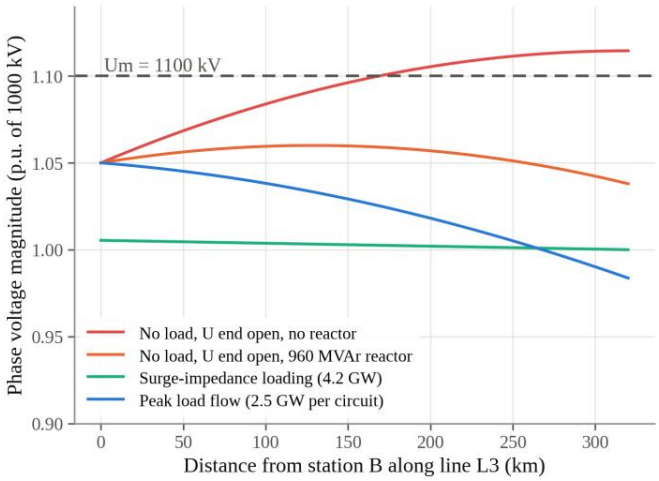


Figure 6: Voltage Z the 320-km Feeder L3: Open Line without and with the 960-Mvar Reactor, at Surge-Impedance Loading, and in the Peak Load Flow

4.1.4. Loadability: The power–angle relation of the lossless line,

$$P = \frac{\text{SIL}}{\sin\beta l} \cdot \frac{V_S V_R}{U_n^2} \sin\delta, \qquad (27)$$

gives a steady-state limit of 4203/0.335=12,540 MW for a 320-km feeder between stiff buses; the 1.2-SIL planning value of (2) corresponds to an angle of about 24° across the line. The definitive limits follow from the P–V and stability studies.

4.1.5. 420-kV Feeders: Each 420-kV circuit is a quad bundle of ACSR "Moose" (31.77 mm) with 450-mm spacing on double-circuit towers. Its parameters are R_1 / X_1 = 0.0175/0.2528 Ω/km, C_1 = 14.43 nF/km, Z_c = 236.2 Ω and SIL = 678 MW; its thermal rating at 85 °C and 50 °C ambient is 3326 A (2305 MVA), and the surface-gradient ratio is 0.64. The feeders carry 897–1617 A at peak and at most 2223 A after the loss of another circuit, 67% of the thermal rating.

5. Configuration and Single Line Diagrams

5.1.1100-kV Switchyard

The 1100-kV switchyard is a fully gas-insulated one-and-a-half-breaker arrangement with two GIL main busbars rated 8000 A and 63 kA/3 s (Figure 7; the two full-page single-line diagrams are placed at the end of the paper). Five diameters are equipped with three breakers each (15 breakers) and space is reserved for a sixth. Diameters D1–D4 each carry one line and one bank (L1/T1 to L4/T4) and D5 carries T5 and the reserved line position. Pairing a line with a bank in every diameter means that a center-breaker failure removes one line and one bank rather than two lines or two banks, which keeps the post-fault network balanced. Every diameter item is rated 6300 A, which covers the worst diameter throughput found in the contingency study (a line at 3005 A plus a bank at 1732 A). The detailed diagram of diameter D1, with its line entrance, bank, tertiary plant and 420-kV incomer, is Figure 8.

5.2. 420-kV Switchyard and Automatic Reconfiguration

At 420 kV a gas-insulated double busbar with one breaker per circuit is divided into four sections S1–S4 (Figure 9), each with a bus coupler, joined by normally open bus-section breakers on both busbars; with the incomers, feeders, STATCOM and capacitor bays this gives 38 breakers. Sectionalizing is imposed by the fault level: with an infinite 1100-kV source each bank contributes 24.0 kA to a 420-kV fault, and coupling all sections in the ultimate network would give 83.3 kA (Section VII). Banks T1 and T2 feed S1, and T3, T4 and T5 feed S2, S3 and S4.

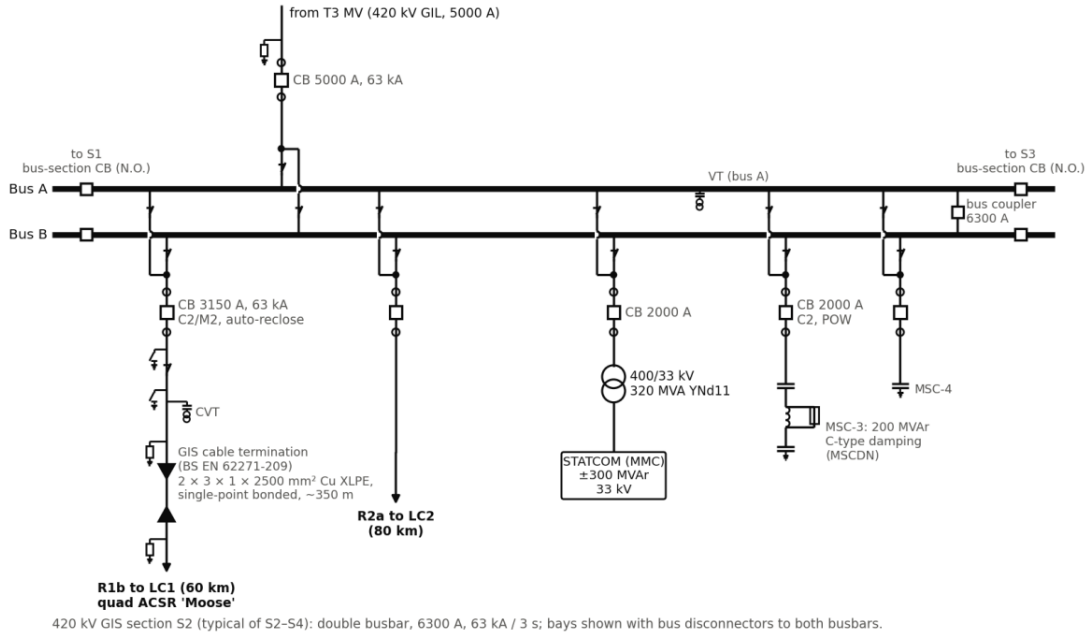


Figure 9: Single-Line Diagram of a 420-kV GIS Section (S2, typical of S2–S4): Double Busbar with Bus Coupler, Bank Incomer by 420-kV GIL, Outgoing Feeders with XLPE Cable Connections, STATCOM and MSCDN bays

Because five banks feed four sections, the loss of T1 (or T2) would leave its partner at 100.8% loading. An automatic bus-section reconfiguration (ABR) scheme therefore closes predefined bus-section breakers within 1 s of a bank trip (Table 5), subject to a real-time fault-level check by the substation automation system that blocks any closure placing more than two banks on a coupled group.

Bank lost	Breakers closed	Worst bank loading	Ultimate $I''k_3$
T1, T2 or T3	S1–S2	90.0%	58.9 kA
T4 or T5	S2–S3, S3–S4	91.9%	57.5 kA

Table 5: Automatic Bus-Section Reconfiguration

5.3. Transformer Banks

Each bank comprises three single-phase autotransformers connected YNa0d11 (Figure 10), with ONAN/ONAF/OFAF cooling at 60/80/100%, guaranteed losses of 200 kW (no-load) and 600 kW (load) per unit, and insulation levels of 2400/1800 kV (lightning/switching impulse) at the HV terminal. The neutral is grounded through a 10-Ω reactor and insulated for U_m = 170 kV (Section VII); the tertiary carries a 240-Mvar shunt reactor, four 60-Mvar detuned capacitor steps and a station-service transformer.

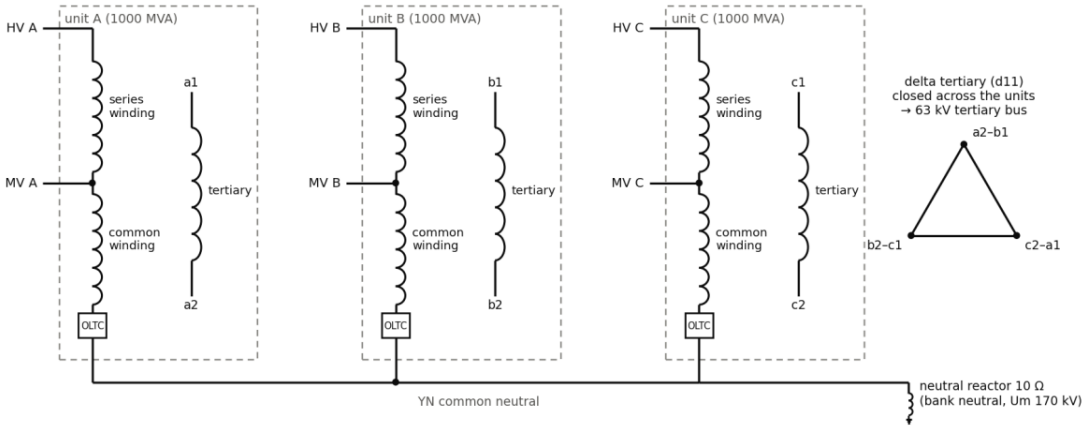


Figure 10: Connection of One Bank: Three Single-Phase Autotransformers with Series and Common Windings, Neutral-End OLTC, Delta Tertiary Closed Across the Units, and Common Neutral Grounded Through the 10-Ω Reactor

5.4. Reliability of the Switching Arrangement

The candidate 1100-kV arrangements were compared with the reliability model of Section III-G using breaker active-failure rates, busbar fault rates, stuck-breaker probabilities and repair and maintenance times typical of UHV GIS. The results (Table 6, Figure 11) show that the double busbar with single breakers is decisively inferior, because every breaker repair (336 h) removes its circuit and a busbar fault removes half of the circuits until disconnector switching is complete. The one-and-a-half-breaker arrangement produces no expected curtailment: its most frequent multiple-circuit event, a center-breaker active failure (0.02 occ/yr), removes one line and one bank, which the remaining plant can carry, and the diameters remain self-supporting even if both busbars are lost. The double-breaker arrangement reduces multiple-circuit events further but costs three more UHV breakers and, with both busbars out, isolates every circuit.

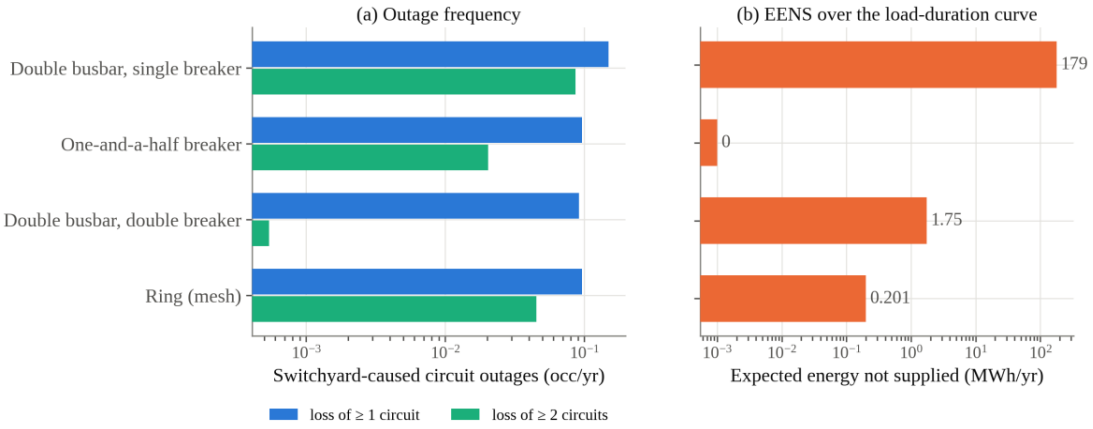


Figure 11: Switchyard-Caused Reliability of the Candidate 1100-kV Arrangements: (a) Outage Frequency; (b) Expected Energy not Supplied Over the Load–Duration Curve

Arrangement	CBs	≥1 circuit (occ/yr)	≥2 circuits (occ/yr)	EENS (MWh/yr)
Double busbar, single breaker	10	0.149	0.086	179
One-and-a-half breaker	15	0.096	0.020	0.0
Double busbar, double breaker	18	0.091	0.0005	1.7
Ring	9	0.096	0.045	0.20

Table 6: Reliability of 1100-KV Switching Arrangements

6. Flow, Contingency and Voltage Stability

6.1. Peak Load

The 24-bus network was solved with the hub voltages held at 1.05 p.u., the regional grid at 1.00 p.u. and the STATCOM-equipped sections at 1.01 p.u., with load-center demands at 0.95 power factor scaled so that exactly 10,000 MW is delivered at the 420-kV busbars (Figure 2). The 1100-kV busbar operates at 0.984 p.u. and −9.8°, the four 420-kV sections at 1.002–1.010 p.u. and the load centers at 0.969–0.979 p.u. The feeders deliver 10,007 MW: 2520 MW over each 280-km circuit (loss 15.5 MW) and 2483 MW over each 320-km circuit (loss 16.8 MW). The five banks carry 1966–2071 MW each, a loading of 66.1–69.7% of 3000 MVA, with on-load tap changers at +2 steps; the twelve 420-kV feeders carry 606–1081 MW and deliver 2533 Mvar at a power factor of 0.969. Total network losses are 154.3 MW.

6.2. Reactive Power Balance

Table 7 sets out the reactive balance at peak. Three sinks dominate: the fixed line reactors at the substation absorb 3370 Mvar at the operating voltage, the banks with their 18% impedance consume 1567 Mvar, and the regional load draws 2533 Mvar. A plant consisting of tertiary capacitors (1200 Mvar) and STATCOMs (±900 Mvar) alone the usual deterministic provision proved insufficient: the STATCOMs were driven to their 300-Mvar limits in steady state, leaving no dynamic reserve, and the 1100-kV busbar fell to 0.971 p.u. (Table 8). Two 200-Mvar mechanically switched capacitor banks with C-type damping networks (MSCDN) per section, 1600 Mvar in total, return the STATCOMs to 36, 74 and 155 Mvar with only half the tertiary steps in service, and reduce the losses by 8 MW and the hub reactive outputs by 381 and 337 Mvar.

Item	Mvar
Net import from the UHV feeders (after the 3370 Mvar absorbed by the line reactors)	+1543
Tertiary capacitors, 2 × 60 Mvar per bank	+665
Reactive consumption of the five banks	−1567
420-kV MSCDN, 8 × 200 Mvar	+1626
STATCOMs (steady state)	+265
Delivered to the twelve feeders (p.f. 0.969)	2533

Table 7: Reactive-Power Balance at Peak (Mvar)

Plant	U (p.u.)	Lowest LC (p.u.)	STATCOM S2/S3/S4 (Mvar)	Losses (MW)
Tertiary C (2 steps) + STATCOM	0.971	0.950	300/300/300	162.3
Tertiary C (4 steps) + STATCOM	0.976	0.968	277/300/300	156.7
+ 1 × 200 Mvar MSC per section	0.981	0.965	300/300/300	155.7
+ 2 × 200 Mvar MSC per section (adopted)	0.984	0.969	36/74/155	154.3

Table 8: React Plant Alternatives at 10 GW

At the design-margin load of 11,000 MW the banks are loaded at 72.9–76.7%, and with all four tertiary steps in service the STATCOMs return to −7, 41 and 125 Mvar and the tertiary voltage rises to 1.113–1.132 p.u., within the 72.5-kV highest voltage. At 3000 MW, with all capacitors out, the 1100-kV busbar rises to 1.015 p.u. At a 1000-MW valley the three STATCOMs would saturate at −300 Mvar without the five 240-Mvar tertiary reactors; with them the sections are held at 1.009–1.010 p.u. and the 1100-kV busbar at 1.035 p.u., which sizes the tertiary reactors.

6.3. Contingencies

All 22 single contingencies each UHV feeder, each bank, each 420-kV feeder and one Statcom were simulated at 10 GW (Figure 12). The loss of a UHV feeder is the most onerous for reactive power: the 1100-kV busbar falls to 0.970 p.u., the parallel circuit carries 5044 MW (1.20 SIL, 3005 A), and the STATCOMs approach their limits until the remaining tertiary steps are switched in. The loss of bank T1 without corrective action would load T2 to 100.8%; with ABR the worst bank loading is 90.0% (T1–T3 outages) and 91.9% (T4 or T5). The worst 420-kV feeder current, 2223 A (R1b after the loss of R2a), is 71% of the 3150-A bay rating, and the lowest load-center voltage, 0.951 p.u., follows the loss of R4b. No contingency violates a thermal or voltage limit. The simultaneous loss of T1 and T2 (N-2), with all bus sections coupled, leaves three banks at 113.4% (10 GW) or 126.1% (11 GW); its thermal consequence is assessed in Section XI.

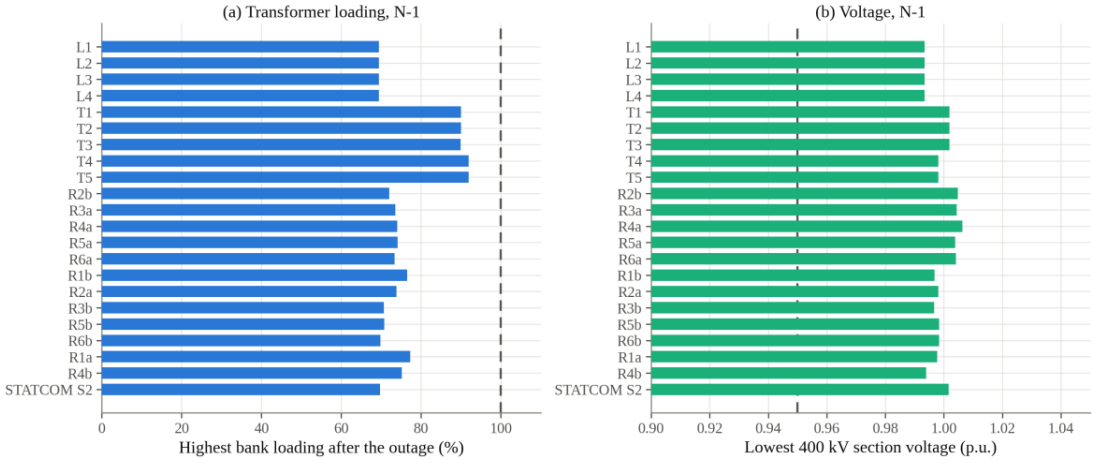


Figure 12. N-1 Screening at 10 GW with Automatic Bus-Section Reconfiguration: (a) Highest Bank Loading; (b) Lowest 420-Kv Section Voltage After Each Single Contingency.

6.4. Voltage Stability

P–V curves were traced by increasing the load-center demands with the additional generation shared between the hubs (Figure 13). The maximum deliverable power is 15.5 GW intact, 13.8 GW with a 320-km feeder out and 12.1 GW with the whole of corridor B out, i.e., margins of 55%, 38%

and 21% over the design load, well above the 5–10% post-contingency margin commonly required. The nose voltages are high (0.79–0.84 p.u.), typical of heavily compensated systems, so voltage magnitude alone is a poor indicator of proximity to collapse; the STATCOM reactive reserve is monitored instead.

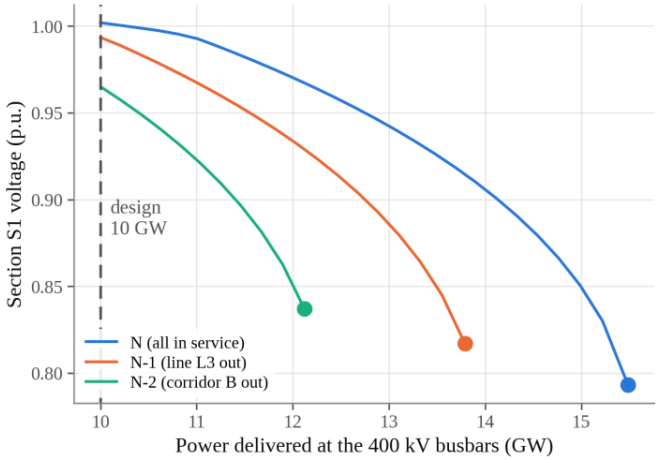


Figure 13: P–V Curves at 420-kV Section S1 for the Intact Network, with one 320-km Feeder Out, and With Corridor B Out

7. Short Circuit and Neutral Grounding

7.1. Fault Levels

Two network states were studied. The present network is the 24-bus model of Section VI. In the ultimate network a future infeed is added at the 1100-kV busbar and sized so that the three-phase fault there equals the 63-kA breaker rating, the only defensible statement of the fault level the substation must withstand over its life:

$$z_{\text{ult}} = \frac{c\, S_B}{\sqrt{3}\, U_n I''_{k,r}} = 0.01008$$

$$z_{\text{add}} = \left(z_{\text{ult}}^{-1} - z_{\text{pres}}^{-1}\right)^{-1} \tag{28}$$

which gives z_{add} =0.0161 p.u. with an assumed X/R ratio of 32. The fault levels are listed in Table 9 and plotted in Figure 14.

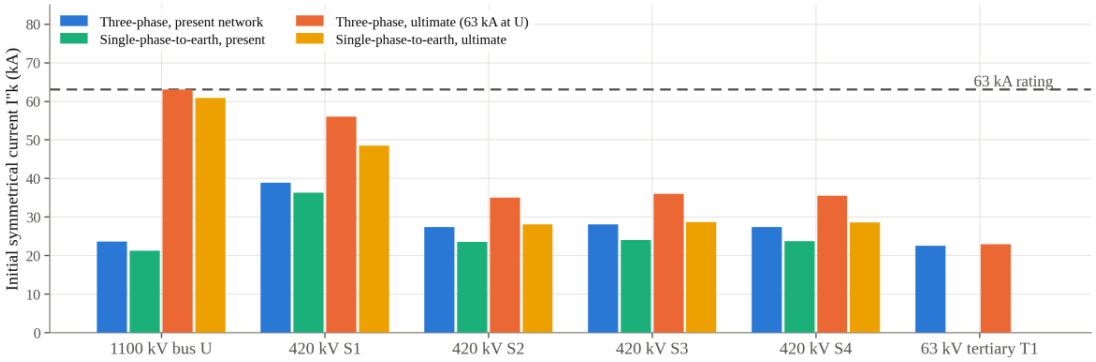


Figure 14: Three-Phase and Single-Phase-to-Ground Short-Circuit Currents in the Present and Ultimate Networks, Compared with the 63-kA Rating

Busbar, network	I''_{k3} (kA)	I''_{k1} (kA)	X_0/X_1	τ (ms)	i_p (kA)
1100 kV U, present	23.6	21.2	1.33	109	64.0
1100 kV U, ultimate	63.0	60.9	1.10	104	170.6
420 kV S1, present	38.8	36.3	1.20	104	105.0
420 kV S1, ultimate	56.0	48.4	1.46	119	152.3
420 kV S2–S4, ultimate	35.0–36.0	28.1–28.7	1.72–1.76	104–106	94.9–97.4
63 kV tertiary, ultimate	18.9–22.9	–	–	277–422	52.6–63.9

Table 9: Initial Symmetrical Short-Circuit Currents (Voltage Factor 1.1, 10-Ω Neutral Reactors)

7.2. Why the Single-Phase Fault Governs at 420 kV

For $R \ll X$ and $k = X_0 / X_1$, (15) gives

$$\frac{I''_{k1}}{I''_{k3}} = \frac{3}{2 + k}, \tag{29}$$

so, the single-phase fault exceeds the three-phase fault wherever $k < 1$. Seen from a 420-kV busbar, the positive-sequence path is $z_H + z_M = 0.066$ p.u. per bank in series with the 1100-kV system, whereas in zero sequence the delta tertiary closes a parallel path $z_M + z_T$ = -0.088 + 0.528 = 0.440 p.u., and the negative MV branch of the autotransformer lowers the impedance further. With two banks on S1 and solidly grounded neutrals, $k \approx 0.66$ in the ultimate network, and the single-phase fault at S1 reaches 63.0 kA—the full switchgear rating with no margin. A deterministic assessment by the three-phase value (56.0 kA) would not have revealed this.

7.3. Neutral Reactor Selection

A reactor Z_n in each bank neutral modifies the zero-sequence branches as in (13). With n = 2.5 and Z_n = 10 Ω (0.0625 p.u. on the 400-kV base),

$$\Delta Z_{H0} = -j0.0450, \quad \Delta Z_{M0} = +j0.1125$$
$$\Delta Z_{T0} = +j0.0750 \tag{30}$$

p.u., so that the MV-to-tertiary path, which carries most of the zero-sequence current for a 420-kV fault, is lengthened by the full $3Z_n = j0.1875$ p.u. (Table 10). About 5 Ω would already bring the single-phase fault below the three-phase level. A 10-Ω reactor is selected because it reduces the single-phase fault to 48.4 kA, so that the 56.0-kA three-phase fault governs with an 11% margin to the rating, and it nearly halves the neutral current, while the neutral voltage of 101 kV stays well inside a neutral insulated for U_m = 170 kV (325-kV short-duration and 750-kV lightning withstand). Beyond 10 Ω the returns diminish: 20 Ω lowers the fault by only a further 5.5 kA but raises the neutral voltage to 140 kV and the earth-fault factor at 420 kV. The neutral arrester (U_r = 192 kV) does not conduct at the 101-kV neutral voltage.

Z_n (Ω)	I''_{k1} at S1 (kA)	Margin to 63 kA	Neutral current (kA)	Neutral voltage (kV)
0	63.0	0.0%	18.4	0
5	53.6	14.9%	13.0	65
10	48.4	23.2%	10.1	101
15	45.2	28.3%	8.3	124
20	42.9	31.9%	7.0	140

Table 10: Effect of the Neutral Reactor (Ultimate Network)

With the reactor s in service the earth-fault factor,

$$k_e = \frac{\sqrt{3}\sqrt{k^2 + k + 1}}{k + 2}, \tag{31}$$

is 1.05 at 1100 kV in the present network (k = 1.33), 1.02 in the ultimate network and at most 1.12 at the 420-kV sections ($k \le 1.76$), so both systems remain effectively grounded. The 420-kV sections must never be operated fully coupled, which would give 83.3 kA; the ABR states of Table 5 reach at most 58.9 kA (three-phase, which governs).

7.4. DC Component and Breaker Duties

The X/R ratios of 31–37 give dc time constants of 98–119 ms, more than twice the 45-ms standard value of IEC 62271-100 [38]. For a 40-ms contact-separation time the dc component is

$$\frac{i_{dc}(t_{op})}{\sqrt{2}\, I''_k} = e^{-40/120} = 71.7\% \ \left(\text{vs. } e^{-40/45} = 41.1\%\right), \tag{32}$$

so the 1100-kV and 420-kV breakers are specified for τ = 120 ms (Fig. 15). The peak factor κ = 1.914 at the ultimate 1100-kV busbar gives i_p = 170.6 kA, a ratio of 2.71, which exceeds the standard 2.5 and marginally exceeds 2.7; the 1100-kV peak withstand is therefore specified as 171 kA. The 63-kV tertiary breakers see X/R ratios of 87–132 and dc time constants of 277–422 ms and are verified by generator-duty test methods.

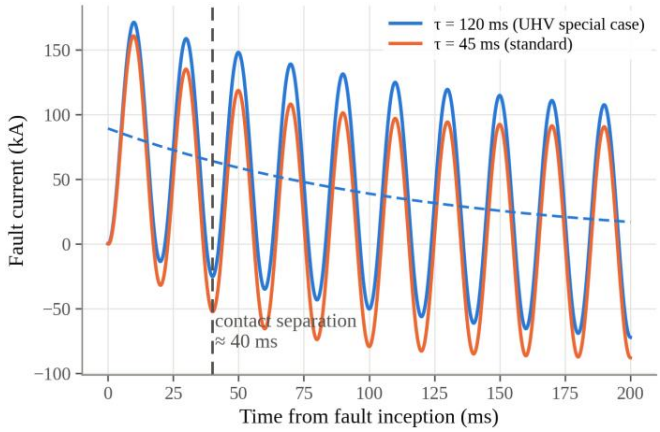


Figure 15: Fully Offset 63-kA Fault Current at 1100 kV for Dc Time Constants of 120 ms and 45 ms; the Dc Component at 40-ms Contact Separation Rises from 41% to 72%

7.5. Ground-Fault Current Distribution and Mechanical Effects

For a ground fault at the 1100-kV busbar, part of the fault current returns through the bank neutrals, which are bonded to the grid and produce no ground potential rise, and the rest leaves through the soil, ground wires and cable screens to remote sources. Because the effectively grounded 400-kV network behind the banks is a strong zero-sequence source, the neutral currents reverse—they flow from the windings *into* the grid (10.1 kA present, 9.0 kA ultimate)—and the grid must discharge 31.3 kA (present) or 69.8 kA (ultimate) to remote sources, more than the fault current itself (21.2 and 60.9 kA). This autotransformer property [23] is missed when the grid current is taken as the breaker rating times an assumed split factor, and it governs the grounding design of Section XIII.

Electrodynamic forces were checked by IEC 60865-1 [39]. The 1100-kV flexible line-entrance span (8 × ACSR 630/45, 15-m phase spacing) sees 39.7 N/m at 63 kA, a swing-out of 14°, and a bundle pinch force of 609 N/m per subconductor; the 420-kV tubular busbars (Al 160 × 10 mm, 12-m span) reach 54.6 MPa, 25% of the permissible stress; the single-phase GIL, with 90–95% enclosure return current, sees only 8–34 N/m.

8. Transient Stability

8.1. Study Cases and Clearing Times

Each hub is a 4.5-s classical machine of 7300 or 6700 MVA with X'_d=0.35 p.u. including its step-up transformer, exporting 5072 MW (hub A) and 5000 MW (hub B); the regional grid has 150 s on 1000 MVA. The classical model omits excitation and governor control and is conservative for the first swing. Single-phase faults are cleared by removing the faulted line entirely, i.e., single-pole reclosing is not credited. The clearing times derive from the protection and switchgear: main protection 20 ms, trip relay and two-cycle breaker 40 ms and teleprotection margin 20–40 ms give 80–100 ms for normal clearing; a stuck breaker adds a 50-ms breaker-failure timer and 40 ms for the adjacent breaker, 150 ms in total. The CCTs are listed in Table 11.

Case	Fault and post-fault network	3-ph (ms)	1-ph (ms)	Applied (ms)
F1	At U on L1 (280 km), L1 tripped	143	447	100
F2	At U on L3 (320 km), L3 tripped	137	438	100
F3	1100-kV busbar, no circuit lost	189	553	100
F4	F1 + stuck center breaker: L1 and T1 lost	108	357	150
F4′	F4 with 1.1-GW generation rejection	166	–	150
F5	At S1 on R3a, R3a tripped	227	771	100
F6	At S1, bank T1 tripped	204	715	100

Table 11: Critical Clearing Times of Three-Phase and Single-Phase Faults

8.2. Results and Generation Rejection

With 100-ms clearing, three-phase faults at the substation end of the 1100-kV lines have CCT margins of 37–43% (89% for a busbar fault), and faults on the 420-kV side more than 100%; single-phase faults, more than 90% of UHV line faults, have CCTs of 357–771 ms and are not a stability concern (Figure 16(a)). At 5 ms beyond the CCT both hubs pull out together against the regional grid (Figure 16(c)), the classical first-swing loss of synchronism of a remote generation group.

The breaker-failure case is decisive. If the center breaker of

diameter D1 fails to clear a fault on L1, the breaker-failure protection also removes bank T1; the CCT falls to 108 ms, below the 150-ms breaker-failure clearing time. Without remedial action a three-phase fault with a stuck center breaker would cause loss of synchronism of the generation hubs. The breaker-failure time cannot be shortened safely, because its timer must exceed the breaker's own interrupting time with margin. Rejecting one 1100-MW unit at the hub feeding the faulted corridor at the instant of breaker-failure clearing—sized by the equal-area criterion and confirmed by a simulation sweep—raises the CCT to 166 ms, 11% above the clearing time (Figure 16(b)). The scheme is initiated by the breaker-failure trip of any center breaker coincident with a multiphase fault, sent over two diverse channels within 20 ms, armed when the corridor transfer exceeds 3000 MW, and requires the regional system to carry 1.1 GW of spinning reserve. A detailed study with sixth-order machines, exciters and STATCOM controls should precede implementation and would be expected to lengthen the CCTs, but hardly by the 42 ms needed to reach the 150-ms clearing time.

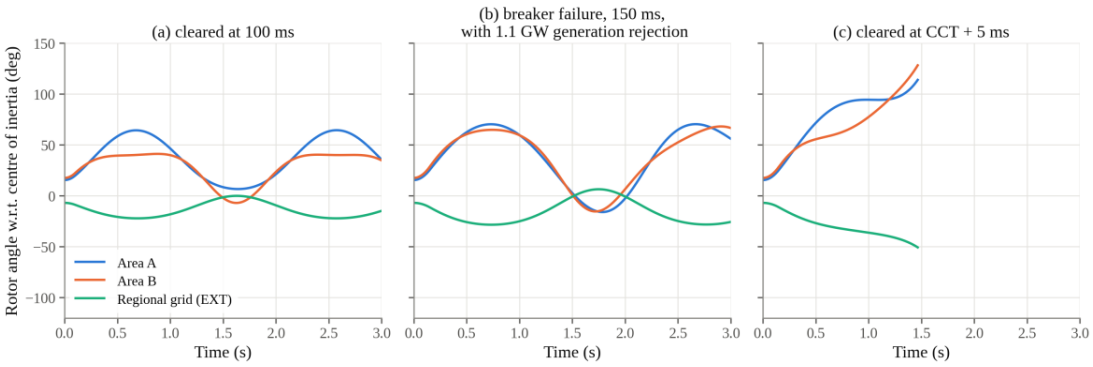


Figure 16: Rotor Angles Relative to the Center of Inertia: (a) Three-Phase Fault on L1 Cleared in 100 ms; (b) Breaker Failure Cleared in 150 ms with 1.1-GW Generation Rejection at hub A; (c) Fault Cleared 5 ms After the CCT

9. Insulation Coordination and Electromagnetic Transients

Insulation coordination follows IEC 60071-1 and -2 [29-40], and every representative overvoltage that can be simulated is obtained from the EMT models of Section III-E, modeled according to IEC TR 60071-4 [8] and the UHV switching guidance of CIGRE TB 570 [5]. The base is 1 p.u. = $1100\sqrt{2}/\sqrt{3} = 898$ kV.

9.1. Temporary Overvoltages and Arrester Rating

The earth-fault factor (31) limits the healthy-phase voltage during a ground fault to 1.05 p.u. If all five banks trip at full load, the busbar remains connected to the hubs through the four lines and their reactors; with the hub machines represented by their EMFs behind transient reactance, the voltage rises to 1.150 p.u. of 1000 kV, i.e., 664 kV rms. The open-line Ferranti rise with reactors (1.060 p.u. of 1000 kV) does not govern. The governing combination is a ground fault during load rejection:

$$U_t = k_e U_{LR} = 1.053 \times 664 = 699 \text{ kV } (\leq 1 \text{ s})$$

$$U_r \geq \max\left(\frac{699}{1.10}, \frac{664}{1.00}, \frac{U_c}{0.8}\right) = 798 \text{ kV}, \quad (33)$$

where 1.10 and 1.00 are the arrester TOV strengths at 1 s and 10 s and $U_c = 638$ kV $\geq U_m / \sqrt{3}$ is the continuous operating voltage. The rated voltage of 828 kV, standard for 1000-kV systems, is therefore set by the continuous stress, not by the TOV. The station arresters at the line entrances, in the GIS line bays and at the transformer and reactor terminals have protective levels of 1460 kV at 2 kA (switching) and 1620 kV at 20 kA (lightning) and a thermal energy rating of 20 kJ/kV (16.6 MJ) [41].

9.2. Slow-Front Overvoltages: Statistical Line Energization

The 320-km line was modeled by three Clarke modes with Bergeron sections and lumped losses at eight points, the 960- and 240-Mvar reactors with their neutral reactor, a coupled R–L source behind the 1100-kV busbar and arresters at both ends (Figure 4(a)); 200 closing operations were simulated for each case (Table 12, Figure 17 and 18). Without mitigation the 2% overvoltage at the open end is 2.50 p.u. (2250 kV). Arresters alone reduce it to 1.62 p.u. at the line ends, but up to 1.92 p.u. remains along the line, which governs the tower clearances, and each operation dissipates up to 7.8 MJ, 47% of the arrester's thermal rating. A 400-Ω pre-insertion resistor with a 10-ms insertion time reduces the 2% value to 1.20 p.u. along the whole line and relieves the arresters almost entirely; controlled closing reduces it further to 1.12 p.u.

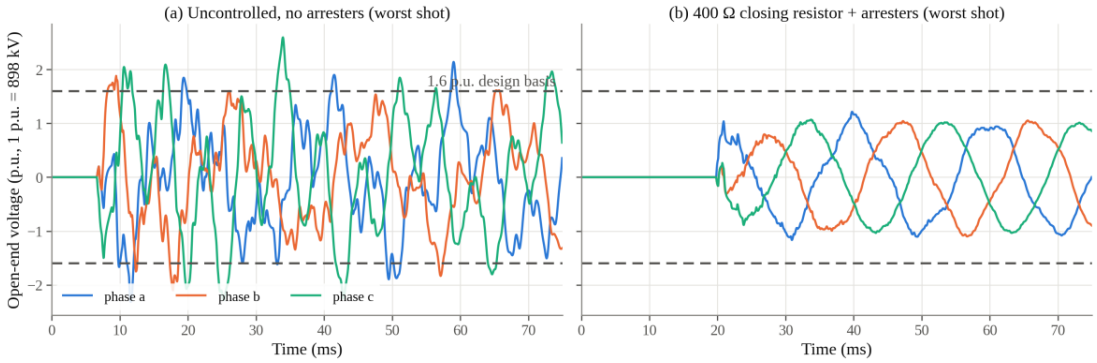


Figure 17: Energization of the 320-km Line: Open-End Phase Voltages for the Worst Closing Operation (a) without Mitigation and (b) with a 400-Ω Closing Resistor and Arresters

Case	Measures	U_{e2} (p.u.)	Max. (p.u.)	Arrester energy
C1	Uncontrolled, no arresters	2.50	2.60	–
C2	Uncontrolled, arresters	1.62	1.64	7.8 MJ
C3	400-Ω resistor, arresters	1.20	1.22	0.04 MJ
C4	Resistor + controlled closing	1.12	1.13	0

Table 12: Statistical Energization Overvoltages, 320-KM Line (200 Shots)

Case C2, with the resistor out of service, is the credible worst case for the apparatus, because a resistor or controller failure must not leave the insulation unprotected. Its 2% value (1.62 p.u., 1455 kV) is capped by the arrester switching protective level (1460 kV = 1.63 p.u.), and the representative slow-front overvoltage is taken as U_{rp}=1.6 p.u. = 1437 kV; the effect of using 1460 kV instead is quantified in Section IX-E. Three-pole reclosing onto trapped charge is excluded by the single-pole reclosing policy (Section XII).

9.3. Fast-Front Overvoltages: Lightning

The station model (Figure 4(b)) represents the last 600 m of line (300 Ω), the line-entrance gantry with its CVT (5 nF) and arrester on a 10-m lead, a 40-m drop to the SF_6/air bushing (1.2 nF), 70 m of GIS line bay, and either the GIS and GIL path to the transformer (50–300 m, 75 Ω, 285 m/μs) with the transformer capacitance (5 nF) and arrester, or an open breaker 15 m from the diameter node. The incoming surge of 4200 kV, representative of a backflash at the first tower, has a front steepness of 2000 kV/μs after corona attenuation and is solved with a 2-ns step. The results (Table 13, Figure 19) establish three design rules. First, the transformer must have its own arrester: without it, reflections on the GIS–GIL path raise its terminal voltage to 2.4–2.9 MV, while with it the voltage is 1.81–1.83 MV, practically independent of the separation distance, which the simplified separation-distance formula cannot capture. Second, an open line breaker doubles the incoming surge and needs a gas-insulated arrester in the line bay at the diameter node; one at the GIS line entrance is marginally insufficient. Third, a lightning withstand of 1950 kV would be inadequate, and 2100 or 2250 kV would leave margins of only 1% and 8%.

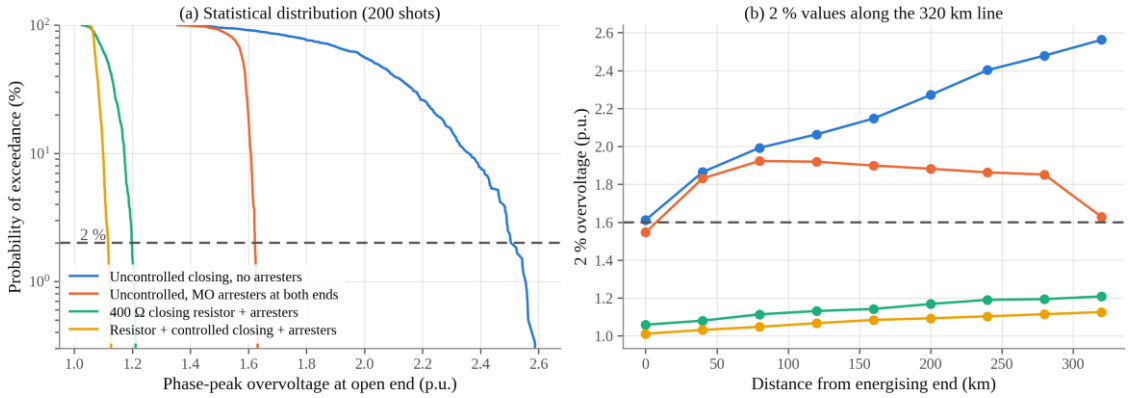


Figure 18: (a) Probability of Exceeding the Open-End Phase-Peak Overvoltage for the Four Mitigation Cases; (b) 2% Overvoltage along the 320-km Line

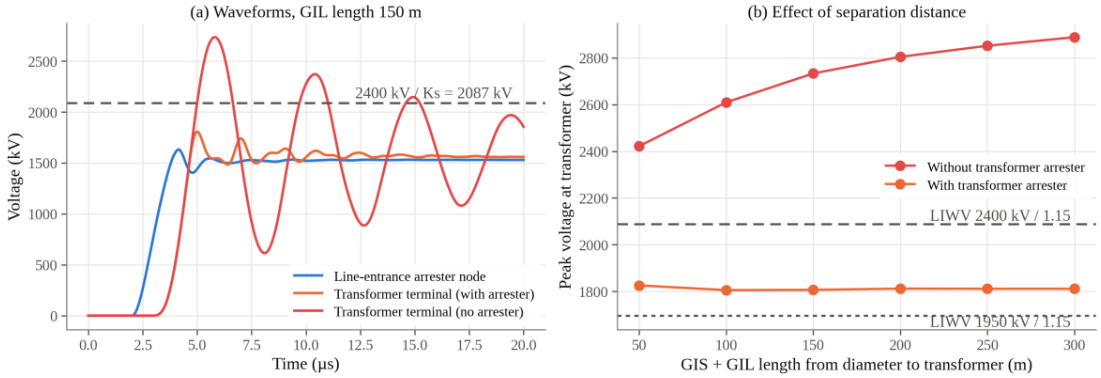


Figure 19: Lightning Overvoltages: (a) Waveforms at the Line-Entrance Arrester and the Transformer Terminal with and Without the Transformer Arrester (GIS + GIL length 150 m); (b) Peak Transformer-Terminal Voltage Versus GIS + GIL Length

Location and configuration	Peak (kV)	Limit (kV)
Line-entrance arrester (gantry)	1631	2087
Transformer, with arrester, 50–300 m	1805–1825	2087
Transformer, no arrester, 50 / 300 m	2422 / 2889	2087
Open breaker, no GIS arrester	3014	2087
Open breaker, GIS arrester at line entrance	2104	2087
Open breaker, GIS arrester in line bay	1631	2087

Table 13: Lightning Overvoltages in the 1100-KV Station

9.4. Very-Fast Transients and Transient Recovery Voltage

A disconnector restrikes with −1-p.u. trapped charge, modeled with a gap resistance collapsing in about 5 ns and the GIS sections as lossless lines, produces a very-fast transient overvoltage (VFTO) of 1.64 p.u. (1470 kV) at an open breaker (1.48 p.u. with −0.5 p.u. trapped charge) [42]. Although this is within the lightning withstand, VFTO stresses GIS and transformer insulation at several megahertz, where the withstand is lower, and reported VFTO-related failures concentrate at 1100 kV [1-43]. A 500-Ω damping resistor in each 1100-kV disconnector limits the VFTO to 1.00 p.u. (Figure 20).

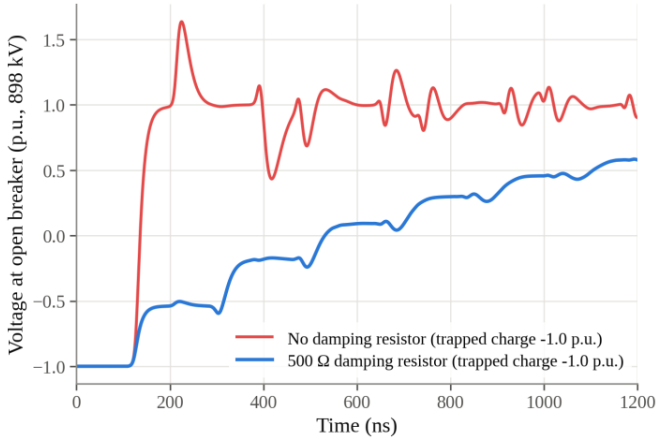


Figure 20: VFTO at an Open Breaker During a Disconnector Restrike with −1-p.u. Trapped Charge, without and with a 500-Ω Damping Resistor

The terminal-fault transient recovery voltage (TRV) was computed by current injection at the opened breaker and multiplied by the first-pole-to-clear factor k_{pp} = 1.2. With an amplitude factor k_{af} = 1.5 and a rate of rise of 2 kV/µs, the four-parameter envelope adopted for the 1100-kV breaker is

$$u_c = k_{pp} k_{af} U_r \sqrt{2/3} = 1617 \text{ kV}$$

$$u_1 = 0.75\, k_{pp} U_r \sqrt{2/3} = 808 \text{ kV}$$

$$t_1 = u_1/(2 \text{ kV/µs}) = 404 \text{ µs}, \qquad t_2 = 4t_1 = 1617 \text{ µs}. \tag{34}$$

The simulated TRV for the ultimate 63-kA duty peaks at 1552 kV (amplitude factor 1.44) with a rate of rise of 1.58 kV/µs, and that of the present network (20 kA) at 1584 kV with 0.84 kV/µs; both lie within the envelope (Figure 21).

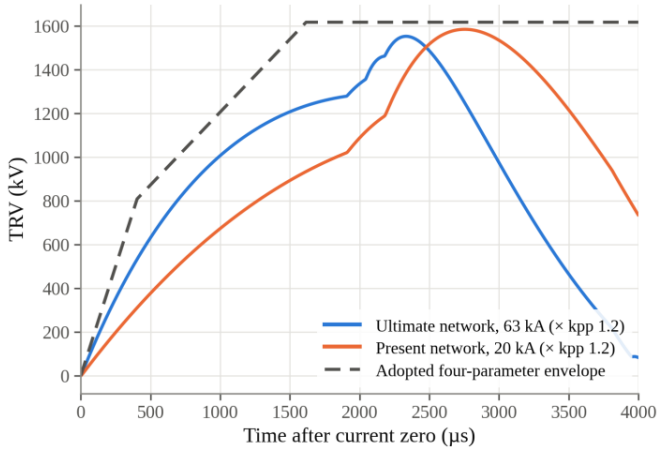


Figure 21: Terminal-Fault TRV of the 1100-kV Breaker in the Ultimate (63 kA) and Present (20 kA) Networks with the Adopted Four-Parameter Envelope

9.5. Selection of Withstand Voltages

The required withstand voltages follow from

$$U_{rw} = K_c\, K_a\, K_s\, U_{rp}, \qquad K_a = e^{mH/8150}, \tag{35}$$

with the coordination factor K_c = 1.05, m = 0.75 (switching) or 1.0 (lightning) at H = 500 m, and safety factors K_s = 1.05 (external) and 1.15 (internal). For the internal lightning withstand, the EMT transformer-terminal voltage (1806 kV at 150 m) replaces the deterministic estimate. Table 14 and Figure 22 show the progression: the selected 1800-kV switching impulse withstand has margins of 8.5% over the external and 3.7% over the internal requirement, and the 2400-kV lightning impulse withstand 15.5% over the governing internal requirement. With U_rp taken as the 1460-kV arrester protective level, the switching margins would be 6.8% and 2.1%, still positive. The protective ratios are 2400/1620 = 1.48 and 1800/1460 = 1.23, above the recommended minima of 1.25 and 1.15 [41].

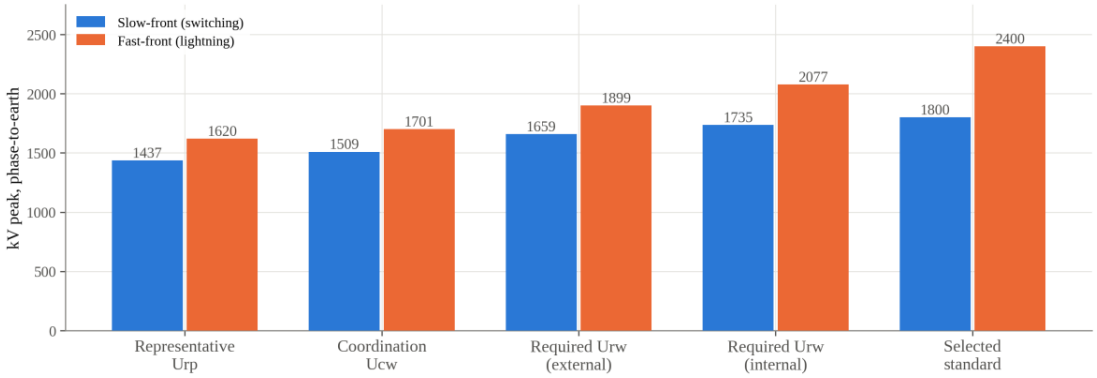


Figure 22: Insulation Coordination at 1100 kV: Progression from the Representative Overvoltages to the Selected Standard Withstand Voltages

Step	Switching impulse	Lightning impulse
U_{rp}	1437 (EMT envelope)	1620 (arrester level)
$U_{cw} = K_c U_{rp}$	1509	1701
K_a (500 m)	1.047	1.063
U_{rw}, external (K_s = 1.05)	1659	1899
U_{rw}, internal (K_s = 1.15)	1735	2077 (EMT 1806 × 1.15)
Selected standard value	1800	2400
Margin	8.5% (ext.), 3.7% (int.)	15.5% (int.)

Table 14: Insulation Coordination at 1100kv (Phase-to-Ground, KV Peak)

9.6. Clearances and Creepage

The outdoor clearances follow from the 50% breakdown voltage of the gap with the gap-factor method,

$$U_{50} = \frac{U_{rw}}{1 - 1.3\sigma}, \qquad d = \frac{1}{0.46}\left[\exp\left(\frac{U_{50}}{1080\,K}\right) - 1\right], \tag{36}$$

with σ = 6% and d in meters. For 1800 kV a gap factor of 1.20, chosen conservatively for conductor–crossarm and conductor–window configurations at the line entrances, gives a phase-to-ground clearance of 7.6 m, and 2880 kV phase-to-phase with K = 1.6 gives 11.1 m (11.3 m adopted); at 420 kV the calculated 3.1 m and 3.7 m are rounded up to 3.2 m and 4.2 m. For pollution class c, the unified specific creepage distance of 34.7 mm/kV gives 22,100 mm for line and post insulators and, with the diameter factor of 1.15 for 600-mm housings, 25,400 mm for bushings and arresters. Silicone housings are specified without any creepage reduction, because desert dust followed by dew can mask their hydrophobicity [44].

10. Connections Gas-Insulated Lines and Power Cables

10.1.1100-kV

No extruded ac cable system is standardized above 500 kV—IEC 62067 [45] ends at U_m = 550 kV—and the highest extruded systems in service are at 500–550 kV [46]. All 1100-kV connections are therefore made by rigid GIL to IEC 62271-204 [10,11,47]: the two main busbars (8000 A), the line entrances (6300 A), the transformer connections (4000 A) and the reactor connections, 9.3 km single-phase in total. The insulating gas is a 20/80% SF_6/N_2 mixture at 0.7 MPa, which has about 70% of the dielectric strength of pure SF_6 at the same pressure with one fifth of its SF_6 content. For a coaxial conductor of radius R_1 in an enclosure of inner radius R_2,

$$E_{\max} = \frac{U}{R_1 \ln(R_2/R_1)}, \qquad C = \frac{2\pi\varepsilon_0\varepsilon_r}{\ln(R_2/R_1)}$$

$$Z_c = 60\ln(R_2/R_1). \tag{37}$$

For a fixed enclosure the stress is minimized at $R_2 / R_1 = e$. With a 750-mm enclosure, the adopted 300-mm conductor (R_2 / R_1 = 2.5, Figure 23) is within 0.5% of the minimum (Figure 24(a)) and gives 17.5 MV/m at the 2400-kV lightning withstand, 17% below the design limit of 21.2 MV/m (half the critical field of the mixture); the line constants are 60.7 pF/m, 0.183 μH/m and 55.0 Ω, and the charging current is 11.0 A/km.

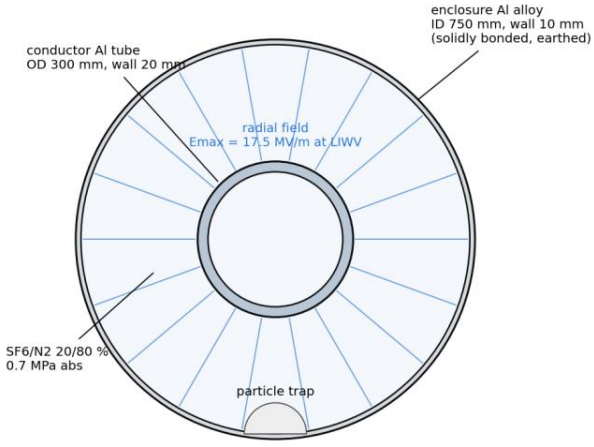


Figure 23: Cross-Section of the 1100-kV GIL: 300 × 20 mm Aluminum Conductor in a 750-mm Aluminum-Alloy Enclosure with SF_6/N_2 (20/80%) at 0.7 MPa

The conductor and enclosure temperatures were computed with the two-node heat balance against limits of 105 °C for silver-plated joints and 70 °C for an accessible enclosure (Table 15, Figure 24(b)). Both a 12-mm and a 20-mm conductor wall meet the limits, but the 20-mm wall is adopted: it reduces the total loss by 29% and keeps the outdoor enclosure in full sun at 67.5 °C, 2.5 K below the touch limit instead of 0.7 K. Solar gain (308 W/m) exceeds the Joule loss outdoors, so outdoor runs receive a low-absorptivity finish and sunshades where accessible.

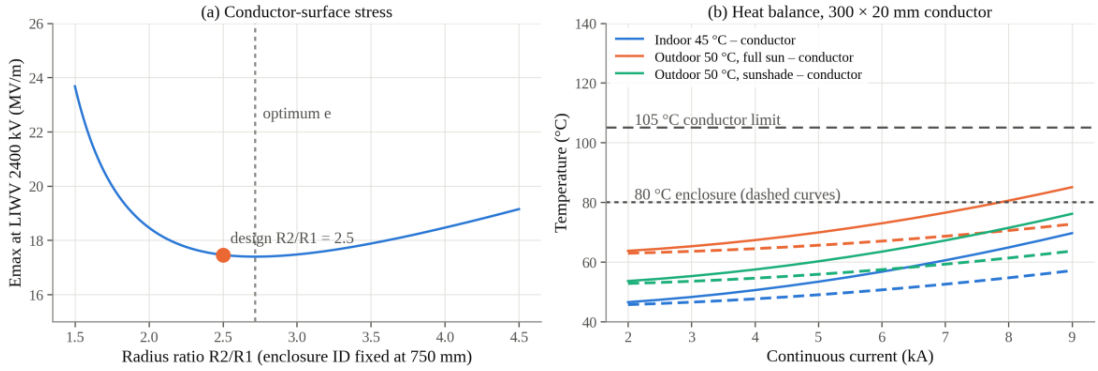


Figure 24: 1100-kV GIL Design: (a) Conductor-Surface Stress at the Lightning Withstand Versus Radius Ratio; (b) Conductor (solid) and Enclosure (Dashed) Temperatures of the 300 × 20 mm Conductor Versus Current

Case	T_c / T_e (°C)	Loss (W/m)
Busbar, 8000 A, indoor 45 °C	64.9 / 54.7	226
Line GIL, 6300 A, 50 °C, full sun	74.0 / 67.5	146
Line GIL, 6300 A, 50 °C, sunshade	64.5 / 58.0	141
Transformer GIL, 4000 A, 50 °C, sun	67.3 / 64.5	58

Table 15: GIL Temperature and Losses Per Phase

10.2.420-kV Transformer Connections: Cable or GIL

Each bank delivers 4330 A at 400 kV continuously and 4910 A in the N-2 emergency. Paralleled trefoil groups of 2500-mm² XLPE cable, rated with the IEC 60287 group calculation at the site conditions (ground 30 °C, dry sand 1.5 K•m/W, thermal backfill 0.8 K•m/W, 1.5-m spacing), give 3374 A with three groups, 4093 A with four and 4704 A with five. Five groups—15 cables and 30 terminations per bank—would be needed for the rated current, and the N-2 current would still exceed the continuous rating. A 420-kV GIL (conductor 180 × 15 mm, 500-mm enclosure) carries the current with one conductor per phase: (37) gives 15.5 MV/m at the 1425-kV lightning withstand, and the heat balance gives conductor/enclosure temperatures of 79.4/69.2 °C at 4330 A in full sun and 84.0/71.1 °C at 4910 A, falling to 75.0/62.0 °C under a sunshade. The transformer connections are therefore made by GIL (3.75 km single-phase) with sunshades.

10.3. 420-kV Feeder Cables

Each outgoing feeder is connected from its GIS bay to the line gantry (about 350 m) by two trefoils of single-core 2500-mm² Milliken copper XLPE cable (27-mm insulation, 11.7 kV/mm at the conductor screen), single-point bonded with sheath voltage limiters. With R_{90} = 1.044 × 10^{-5} Ω/m (skin and proximity factors 0.109 and 0.028), T_1 = 0.413 and T_3 = 0.045 K•m/W and λ_1=0.04, the external thermal resistance of the hottest cable of a group is obtained by superposition of images:

$$T_4 = \frac{\rho_T}{2\pi}\left[\ln\left(u+\sqrt{u^2-1}\right)+\sum_{k\neq p}\ln\frac{d'_{pk}}{d_{pk}}\right] + \Delta T_{bf}, \quad (38)$$

where $u = 2L/D_e$ and $\Delta T_{bf} = N(\rho_{soil} - \rho_{bf})\, G_b / (2\pi)$ corrects for a backfill envelope of geometric factor G_b [33]. The ratings (Table 16, Figure 25) show that the site conditions reduce a single trefoil by 16% relative to temperate assumptions (20 °C, 1.2 K•m/W). Two trefoils 1 m apart are rated 2496 A continuously and 3076 A cyclically (IEC 60853-2), covering the worst N-1 feeder current of 2223 A with 12% and 38% margin; the cable, not the 3150-A bay, is the limiting element of each feeder [48]. The induced standing sheath voltage is 49.8 V/(kA•km), i.e., 22 V at the open end at the 1.25-kA rated current of a cable, and the 300-mm² copper screen exceeds the 121 mm² needed to carry 24.2 kA (half the 48.4-kA single-phase fault at S1) for 0.5 s.

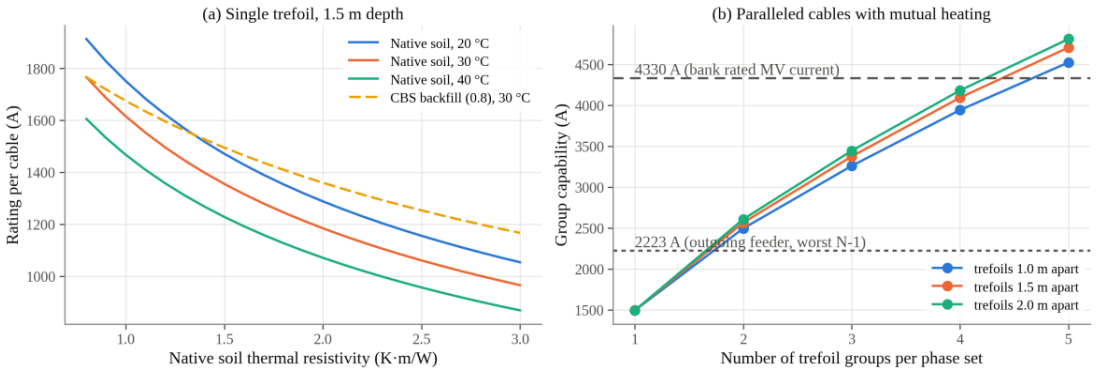


Figure 25: 420-kV Cable Rating: (a) Single Trefoil versus Native-Soil Thermal Resistivity for Ground Temperatures of 20–40 °C and with Backfill; (b) Capability of Paralleled Trefoil groups with Mutual Heating, compared with the Bank Rated Current and the Worst N-1 Feeder Current

Case	Ground, soil	T4 (K•m/W)	Rating
Single trefoil, temperate	20 °C, 1.2	1.89	1623 A
Single trefoil, site, native soil	30 °C, 1.5	2.37	1356 A
Single trefoil, site, backfill	30 °C, 1.5/0.8	1.90	1495 A
Two trefoils 1.0 m apart	30 °C, 1.5/0.8	2.83	2496 A
Two trefoils, cyclic (M = 1.23)	30 °C, 1.5/0.8	–	3076 A

Table 16: Rating of the 420-KV Cable (90 °C, 1.5-m Depth)

11. Transformer Thermal Performance

The model (20)–(22) was integrated with a 1-min step using x = 1.0, y = 1.3, k_{11} = 1.0, k_{21} = 1.3, k_{22} = 1.0, τ_o = 90 min, τ_w = 7 min, R = 3, $\Delta\theta_{or}$ = 45 K and Hg_r = 20 K, so that the rated hot-spot rise of 65 K is 3 K inside the reduced 68-K limit. The ambient follows the design day (35 °C at 05:00 to 50 °C at 15:00) and the load rises from 0.72 p.u. overnight to 1.0 p.u. at 15:30, the air-conditioning peak, so that the load and temperature peaks coincide. The peak bank loadings were taken from the load flow, and the N-1 and N-2 outages were applied at noon after two days of periodic steady state. The results are given in Table 17 and Figure 26.

Condition	Peak K	θ_o max. (°C)	θ_h max. (°C)	Loss of life (days/day)
N, 10 GW	0.697	76.4	88.7	0.03
N, 11 GW	0.767	79.7	93.7	0.05
N-1 with ABR	0.919	87.9	105.7	0.16
N-2, 10 GW	1.134	101.8	125.1	0.95
N-2, 11 GW	1.261	111.4	138.1	2.89

Table 17: Thermal Performance on the 50 °C Design Day

After the loss of one bank, with ABR, the hot spot reaches 105.7 °C, within the 120 °C normal cyclic limit of IEC 60076-7: the N-1 capacity is thermally firm on the hottest day, indefinitely. After the loss of two banks the hot spot exceeds 120 °C 164 min after the event and peaks at 125.1 °C, within the 140 °C long-time emergency limit, with a loss of life of 0.95 day over 24 h; even a 72-h single-phase unit replacement costs only about three days of life. The equal-sharing assessment (128.7%) would have required load shedding; the simulation shows that it is needed only above a peak N-2 loading of K = 1.28, at which the hot spot reaches 140 °C.

12. Reactive Plant, Harmonics and Single-Pole Reclosing

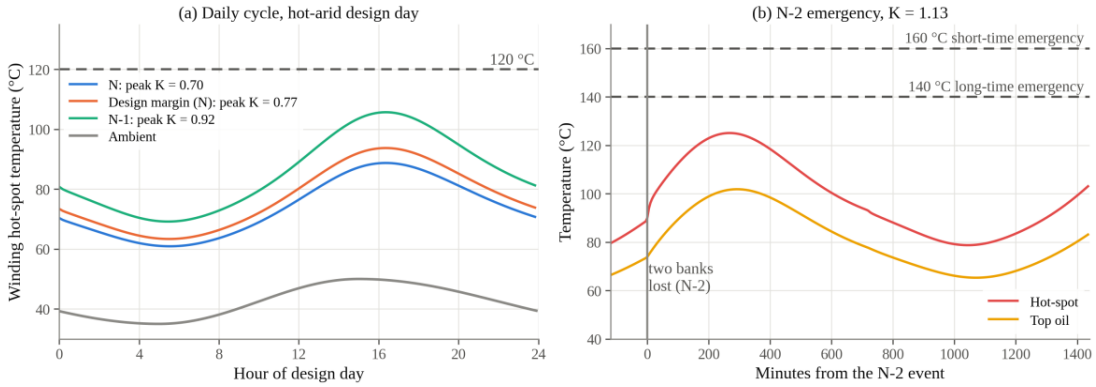


Figure 26: Transformer Thermal Simulation: (a) Hot-Spot Temperature over the 50 °C Design Day in Normal Operation, at the Design Margin and after the Loss of One Bank; (b) Hot-Spot and Top-Oil Temperatures after the Loss of Two Banks at Noon (K = 1.13)

12.1. Reactive Plant

The reactive plant is arranged in four layers with different speeds and purposes (Table 18): fixed line reactors that control the Ferranti rise and support single-pole reclosing; tertiary capacitor and reactor steps switched by the slow voltage control; 420-kV MSCDN for the bulk peak demand; and STATCOMs [49] held near zero output in steady state (at most 155 Mvar at peak) as a dynamic reserve. The slow control switches the steps with 30–60-s delays and a 5-min minimum capacitor off-time; the tap changers are slower still.

Plant	Location	Rating	Function
Line reactors + 420-Ω neutral reactors	1100-kV line entrances	4 × 960 Mvar	Ferranti control, SPAR
Detuned capacitors (6%)	63-kV tertiaries	5 × 4 × 60 Mvar	Peak voltage support
Shunt reactors	63-kV tertiaries	5 × 240 Mvar	Valley overvoltage
MSCDN	420-kV S1–S4	8 × 200 Mvar	Bulk peak support
STATCOM (MMC)	420-kV S2–S4	3 × ±300 Mvar	Dynamic reserve

Table 18: Reactive Plant

12.2. Tertiary Capacitors and Harmonic Resonance

A plain capacitor bank of output Q_c forms a parallel resonance with the network inductance at the harmonic order h_r, and a detuned bank is tuned in series to the order h_t:

$$h_r = \sqrt{S_{sc}/Q_c}, \qquad h_t = 1/\sqrt{p}, \tag{39}$$

where p is the reactor-to-capacitor reactance ratio. The 63-kV tertiary is weak (S_{sc}=2228 MVA, through the high HV–tertiary impedance), so plain 60-Mvar steps would resonate between h = 6.1 (one step) and h = 3.0 (four steps), close to the 5th harmonic of the load. A frequency scan with 6% detuning reactors (h_t = 4.08) moves every resonance below h = 3.5 and reduces the peak impedance by a factor of 4–22 (Figure 27). The residual resonances near the 3rd harmonic (two steps) and 2nd harmonic (three or four steps) are covered by operating rules: balanced triplen harmonics cannot flow into the ungrounded-star banks of the unearthed delta tertiary, and the steps are tripped on loss of voltage and reconnected only 60 s after bank energization, avoiding inrush. The reactors also limit back-to-back inrush to 2.2 kA at 204 Hz instead of 183 kA at 16.7 kHz. Because the capacitor sees $U/(1 - p)$=67.0 kV at 63 kV and 77.1 kV at 72.5 kV, the units are rated 76 kV [50], i.e., 82 Mvar nameplate per 60-Mvar step.

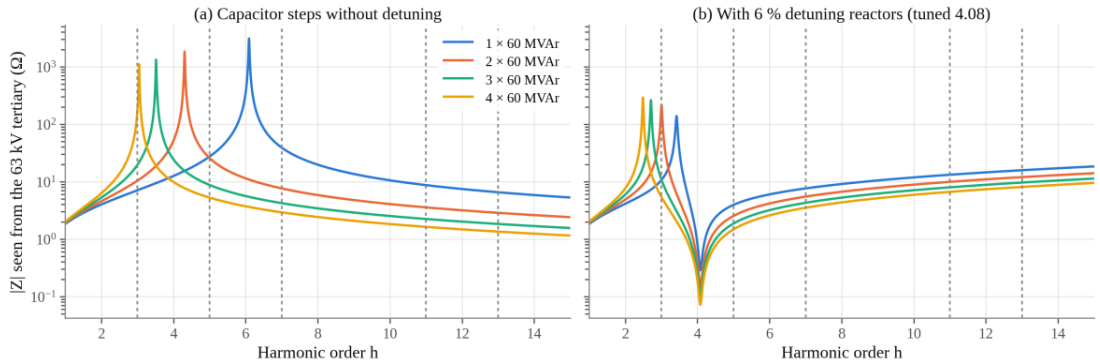


Figure 27: Impedance Seen from the 63-kV Tertiary with One to Four 60-Mvar Steps: (a) Plain Capacitors; (b) with 6% Detuning Reactors

12.3. Single-Pole Reclosing and the Line Neutral Reactor

More than 90% of UHV line faults are single-phase and transient, so single-pole auto-reclosing (SPAR) is applied. With the faulted phase open at both ends, the arc is still fed through the interphase capacitance $C_m = (C_1 - C_0)/3 = 2.03$ nF/km, giving secondary arc currents above 100 A. Kimbark's four-reactor scheme [12-51] neutralizes the interphase capacitance by a reactor in the star point of the line reactors; for perfect compensation,

$$X_n = \frac{X_p^2 B_m}{1 - 3X_p B_m}, \qquad B_m = \omega C_m l, \tag{40}$$

where X_p is the positive-sequence reactance of all line reactors in parallel. Because the two end reactors differ and the line is not perfectly transposed, X_n was selected by a scan of a 20-section coupled π model with faults at both ends and midline (Figure 28, Table 19). Without a neutral reactor the secondary arc current is 107–123 A, and on the 280-km line the open phase resonates with the reactors. The minimum current occurs at about 380 Ω (280 km) and 490 Ω (320 km); a single 420-Ω value keeps both lines clear of their recovery-voltage resonances, limiting the secondary arc current to 21 A and the recovery voltage to 57 kV even at the N-1 transfer, values for which self-extinction within a few hundred milliseconds is reported [1]. A dead time of 1.0 s is specified, with leader–follower reclosing; three-pole reclosing is not used at 1100 kV.

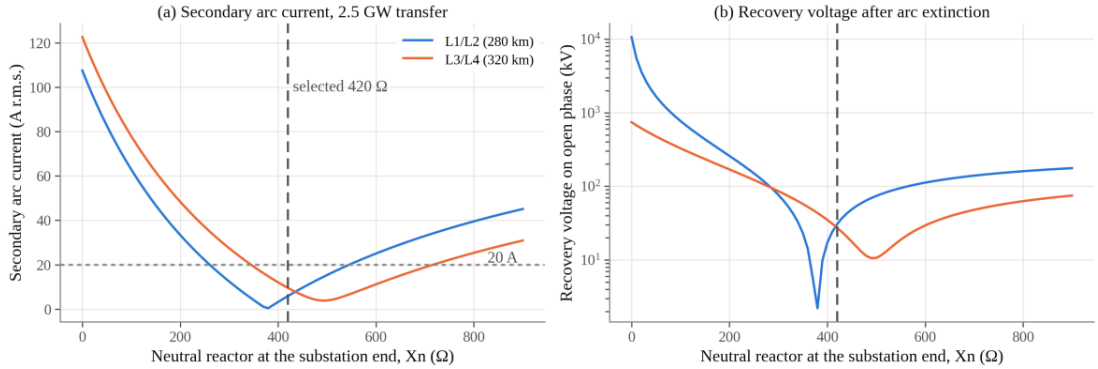


Figure 28: Single-Pole Reclosing on the 1100-kV Feeders at 2500-MW Transfer: (a) Secondary Arc Current and (b) Recovery Voltage Versus the Neutral Reactor at the Substation End

Line	Transfer (MW)	Arc current (A)	Recovery voltage (kV)
L1/L2, 280 km	0 / 2500 / 5000	6.3 / 6.7 / 10.1	33 / 33 / 50
L3/L4, 320 km	0 / 2500 / 5000	10.5 / 14.5 / 21.0	29 / 39 / 57

Table 19: Secondary Arc Current and Recovery Voltage

13. Grounding and Lightning Shielding

13.1. Grid Design and Resistance

The grid is 600 m × 500 m with a 7.5-m mesh of 240-mm² copper at 0.8-m depth and 250 perimeter rods of 15 m (81.3 km of conductor and 3.75 km of rods). The conductor size follows the adiabatic criterion for 60% of the 63-kA fault current for 1.0 s, heated from 50 °C allowing for the hot desert surface to 300 °C, which requires 211 mm². The boundary-element model (24) with eight images gives

$$R_g = 0.168\ \Omega, \tag{41}$$

between the uniform-soil values of 0.083 Ω for ρ_1 and 0.206 Ω for ρ_2 given by Sverak's equation. The two-layer value lies much nearer the value for the 250-Ω•m lower layer: a grid with a 780-m diagonal "sees" soil to a depth comparable with its size, so a design based on the surface resistivity alone would underestimate the resistance and the ground potential rise (GPR) by a factor of two [13-15].

13.2. Current Split and Ground Potential Rise

Of the current I_r = 69.8 kA that the grid must discharge to remote sources (Section VII-E), part returns through the ground wires of the overhead lines and the cable screens. With chain impedances of 1.32 + j0.97 Ω per UHV line and 1.55 + j1.02 Ω per 400-kV line, the parallel return impedance is Z_{eq} = 0.093 + j0.063 Ω, and the split and decrement factors are

$$S_f = \left|\frac{Z_{eq}}{Z_{eq}+R_g}\right| = 0.418$$

$$D_f = \sqrt{1+\frac{T_a}{t_f}\left(1-e^{-2t_f/T_a}\right)} = 1.104 \qquad (42)$$

for T_a = 109 ms and t_f = 0.5 s, so that

$$I_G = D_f S_f I_r = 32.17 \text{ kA}$$

$$\text{GPR} = I_G R_g = 5.42 \text{ kV}. \qquad (43)$$

The ground-wire bonds at the line-entrance gantries are therefore safety-critical connections [52].

13.3. Touch and Step Voltages

With 0.15 m of 3000-Ω•m crushed rock over 100-Ω•m soil (C_s = 0.777) and t_f = 0.5 s, the permissible voltages for a 70-kg person are [52]

$$E_{\text{touch}} = (1000 + 1.5C_s\rho_s)\frac{0.157}{\sqrt{t_f}} = 998 \text{ V}, \qquad (44)$$

and 3327 V for step voltage; EN 50522 ives about 1.2 kV prospective touch voltage with the surface layer and only about 250 V without it [53]. The boundary-element results (Table 20, Figure 29) give a worst touch voltage of 283 V in the corner mesh, 28% of the limit. The IEEE 80 equations give 186 V, an underestimate of 34%, because they assume uniform soil and cannot represent the current concentration at the corners and perimeter rods; the numerical result governs. Outside the grid the surface potential falls steeply, so the security fence is bonded to the grid and placed 1.5 m inside the perimeter conductor, the crushed rock extends 1.5 m outside it, and no grid-bonded metalwork is placed outside the perimeter. With a GPR of 5.42 kV, all signaling leaving the site is optical, and the standby distribution supply enters through an isolating transformer.

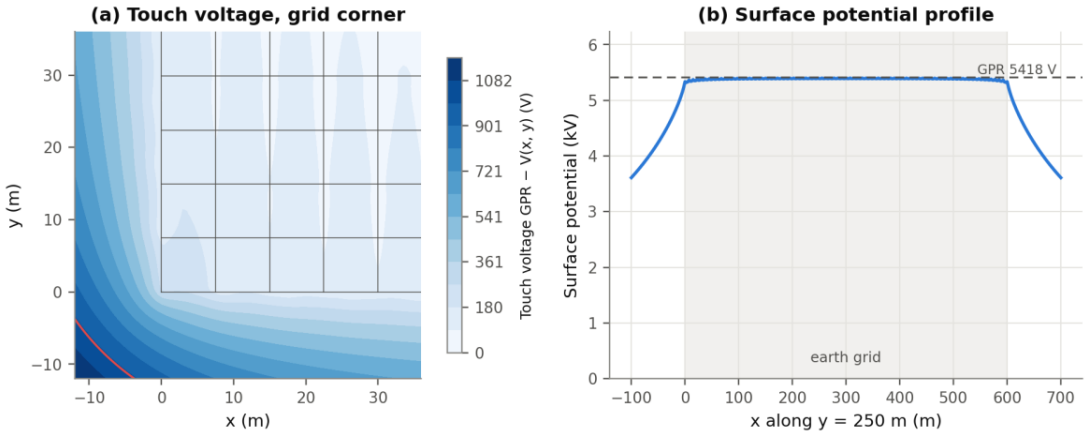


Figure 29: Boundary-Element Results: (a) Touch Voltage GPR – V (x, y) at the Grid Corner with the Permissible-Touch Contour; (b) Surface Potential Along the Grid Center Line

Quantity	BEM	IEEE 80 eq.	Permissible
Touch voltage, corner mesh	283 V	186 V	998 V
Step voltage inside grid	91 V	–	3327 V
Step voltage outside perimeter	114 V	–	355 V

Table 20: Touch and Step Voltages

13.4. Lightning Shielding

The outdoor yards are shielded by masts designed with the electrogeometric model of IEEE Std 998 [54]. The critical stroke current and striking distance for a 2400-kV withstand and a 300-Ω conductor are

$$I_c = \frac{2.2\,\mathrm{BIL}}{Z_0} = 17.6\ \mathrm{kA}, \quad R_s = 8\,k\,I_c^{0.65} = 51.6\ \mathrm{m}, \tag{45}$$

with k = 1, conservative for masts, for which IEEE Std 998 allows 1.2. Masts 45 m high at 58-m spacing give a lowest rolling-sphere point of 36.1 m, 16 m above the 20-m bushing tops; the largest spacing that still protects a 20-m object is 88 m, a 34% margin. Strokes below 17.6 kA can bypass the masts but are limited by the arresters of Section IX.

14. Protection, Automation and Auxiliary Supplies

The substation automation follows IEC 61850 [55] with a process bus (merging units at 4800 samples/s), duplicated station and process networks under the parallel redundancy protocol, and precision time protocol from two GNSS-disciplined grandmaster clocks. Every primary zone has two independent main protections with different principles and manufacturers, separate CT cores, separate dc systems and separate trip coils: line differential and quadrilateral distance with permissive overreach on the 1100-kV lines, duplicated low-impedance busbar differential, and duplicated biased differential plus restricted earth fault on the banks [56].

For the 320-km line L3, the parameters of Table 4 give

$$Z_L = 81.4\angle 88.2^\circ\ \Omega$$

$$k_0 = \frac{Z_0 - Z_1}{3Z_1} = 0.62\angle -13.4^\circ, \tag{46}$$

and the minimum load impedance at the N-1 current of 3005 A and 0.95 p.u. is 183 Ω at up to ±35°. Zones Z1–Z3 reach 85%, 125% and 160% of the line (X = 69.2, 101.7 and 130.2 Ω primary, R = 40, 60 and 80 Ω) with 0, 0.35 and 1.0 s; the largest resistive reach stays about 70 Ω clear of the load region (Figure 30(a)). The transformer differential has a 0.2-p.u. minimum operate current and slopes of 30% and 70% with a breakpoint at 3 p.u. bias; the largest external through-fault (6.5 p.u.) is well inside the restraint region (Figure 30(b)). Because the 104-ms dc time constant drives CT cores into saturation early, a transient simulation of a fully offset 40-kA fault showed that a 600-V knee-point core saturates after 32 ms, whereas the specified 1200-V core is faithful for 90 ms [57]. Breaker-failure protection retrips at initiation and trips the adjacent breakers and the remote end 90 ms later, giving the 150-ms clearance of Section VIII, and initiates the generation rejection.

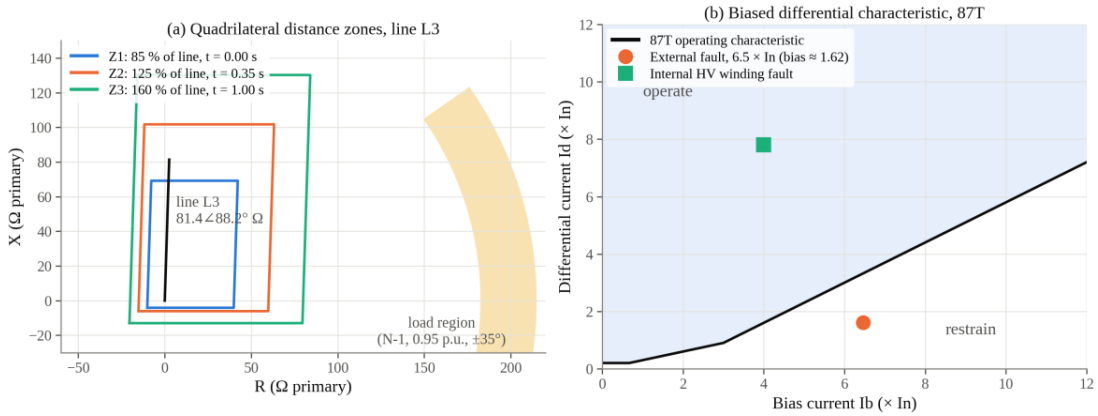


Figure 30: (a) Quadrilateral Distance Zones of Line L3 with the Load Region at the N-1 Maximum Current; (b) Biased Differential Characteristic of the Bank Protection with an External Through-Fault and an Internal Hv-Winding Fault

The auxiliary supply has five sources (Figure 31): three 6.3-MVA, 63/11-kV station-service transformers on the tertiaries of banks on different sections and in different fire zones, a standby distribution-network supply and two 1600-kVA diesel sets. Two independent 220-V dc systems feed main protection 1 and trip coil 1, and main protection 2 and trip coil 2, respectively. Each has a 1500-Ah nickel–cadmium battery sized for an 8-h autonomy, whose governing section sum over the 8-h duty cycle (929 Ah, with 380 A in the first minute for tripping and 245 A in the last minute for closing) is multiplied by temperature, margin and aging factors (1.08 × 1.10 × 1.25), and two 350-A chargers.

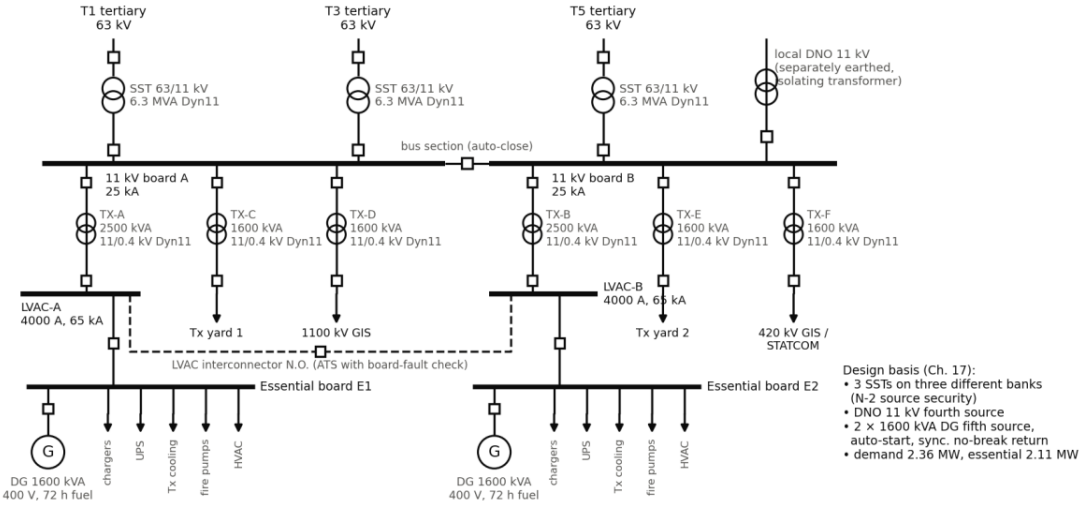


Figure 31: Single-Line Diagram of the Auxiliary Ac System: Station-Service Transformers on Three Bank Tertiaries, Two 11-kV Boards, Standby Network Supply, LV Transformers, Main and Essential Boards, and Diesel Generators

15. Losses and Life-Cycle Economics

15.1. Losses

The losses at 10 GW were assembled from the component models (Table 21). With a loss-load factor of 0.551 for a load factor of 0.73,

$$\eta = \frac{10{,}000}{10{,}017.1} = 99.83\%$$

$$E_{\text{loss}} = 8760\,(P_{\text{fix}} + \text{LLF}\,P_{\text{var}}) = 125.7\ \text{GWh/yr}. \tag{47}$$

The fixed losses (11.0 MW) exceed the load-dependent losses (6.1 MW), and 39% of the losses arise in the reactive plant rather than in the transformation—the cost of controlling the voltage of long UHV lines. The substation losses are small beside the 154 MW of network losses, which therefore dominate the transmission efficiency.

Item	Loss (kW)
Transformer load loss, 5 banks	4105
Line shunt reactors, 4 × 960 Mvar	3370
Transformer no-load loss, 15 units	3000
STATCOMs, 3 × ±300 Mvar	2475
Station auxiliaries (annual average)	2000
1100-kV GIL, 9.3 km	527
Tertiary capacitors and reactors	433
420-kV MSCDN	400
GIS, 420-kV GIL, cables, corona and other	762
Total	17,072

Table 21: Substation Loss Budget at 10 GW

Transformer losses are capitalized for tender evaluation at

$$A = \text{PVF} \cdot 8760\,c_e = 6268\ \text{USD/kW}$$

$$B = A \cdot \text{LLF} \cdot K_p^2 = 1692\ \text{USD/kW} \tag{48}$$

for no-load and load loss, with c_e=60 USD/MWh and the peak loading K_p = 0.70. No-load loss is worth 3.7 times as much per kilowatt as load loss, so tenderers should be steered toward low-loss core steel.

15.2. Switchgear Technology

The life-cycle cost of the 15-breaker 1100-kV switchyard was evaluated for air-insulated (AIS), hybrid (HGIS) and gas-insulated (GIS) switchgear following CIGRE TB 390, with equipment costs of 4.2, 6.7 and 10.0 M USD per breaker position, footprints of 45, 18 and 2.5 ha, maintenance of 1.5, 1.0 and 0.6% per year plus gas management, and the value of

land (Table 22, Figure 32) [58]. AIS is cheapest below a land value of about 84 USD/m^2, HGIS between 84 and 259 USD/m^2, and GIS only above 259 USD/m^2. At desert land values the GIS premium is 42–63 M USD; its selection therefore rests on the risks that the model does not monetize sand and dust on 22–25 m of outdoor creepage, the clearances and fields of a 45-ha AIS yard, and maintenance exposure and HGIS is the principal value-engineering alternative. Controllable shunt reactors in place of fixed line reactors were also evaluated: their net present value is −6.0 M USD at 60 USD/MWh, breaking even at about 74 USD/MWh.

Technology	Excl. land	Land 50 USD/m^2	Land 150 USD/m^2
AIS	101.3	123.8	168.8
HGIS	123.9	132.9	150.9
GIS	164.0	165.3	167.8

Table 22: Life-Cycle Cost of the 1100-KV Switchyard (PV,M USD)

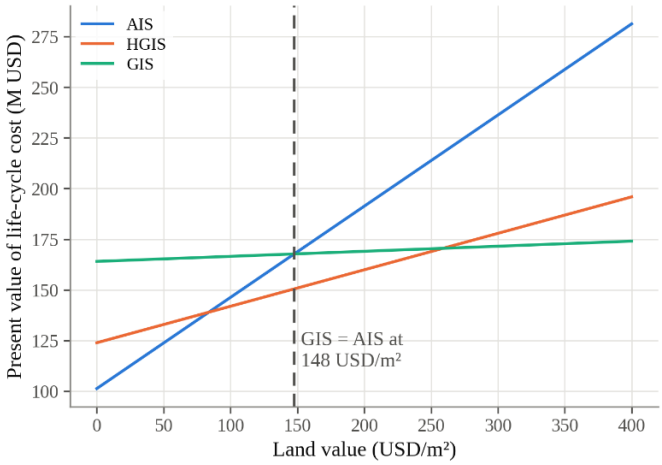


Figure 32: Present value of the 40-year life-cycle cost of the 1100-kV switchyard versus land value for AIS, HGIS and GIS

16. Discussion

16.1. What the Simulations Changed

Table 23 compares the assumptions of a conventional deterministic design study with the results of the simulation-based verification. Three kinds of change can be distinguished. Some deterministic assumptions were unconservative in ways that would have left the plant without margin: the three-phase assessment of the 420-kV fault level, the transformer-connection cables rated for temperate soil, the grid current taken as a fraction of the breaker rating, and the reactive plant sized without a load flow. Some were conservative and would have cost money or led to unnecessary operating restrictions: the equal-sharing N-2 loading and the assumed temporary overvoltage. And some questions are simply invisible to a deterministic study, because they arise from the interaction of the network with the switching arrangement: the breaker-failure stability limit, the unequal loading of five banks on four sections, and the lightning behavior of a GIS–GIL path. I Deterministic Assumptions Versus Simulation-Verified Results

Item	Deterministic basis	Verified result and measure
420-kV fault duty	3-ph, 56.0 kA	1-ph 63.0 kA (solid); NGR 10 Ω → 48.4 kA
Reactive plant	1200 Mvar C + ±900 Mvar STATCOM	STATCOMs saturated; + 1600 Mvar MSCDN
Bank loading, N-1	96.5% (equal sharing)	100.8% without ABR; 91.9% with ABR
Bank loading, N-2	128.7%, load shedding	113.4%; θ_h 125 °C, tolerable
Breaker failure	Not assessed	CCT 108 < 150 ms; 1.1-GW rejection → 166 ms
Lightning protection	Separation-distance formula	Transformer and bay GIS arresters essential
TOV	1.4 p.u. assumed	1.13 p.u. simulated; U_r set by U_c
420-kV transformer link	3 trefoils, 4458 A (20 °C)	3374 A at site; 420-kV GIL adopted
Grid current, GPR	0.35 × 63 kA; 4.5 kV	0.418 × 1.104 × 69.8 kA; 5.42 kV
Switchgear cost	GIS cheapest over life	GIS cheapest only above 259 USD/m^2

Table 23: Deterministic Assumptions Versus Simulation-Verified Results

16.2. Transferability

Several findings are properties of the technology rather than of this site and are likely to recur at other UHV substations. Delta-tertiary autotransformers make the single-phase fault govern on the MV side whenever two or more banks share a busbar, and reverse the neutral current for HV-side ground faults when the MV network is effectively grounded; both effects should be checked by a sequence-network study, and a modest neutral reactor is an effective remedy for the first. One-and-a-half-breaker diameters that pair a line with a bank keep the post-fault network balanced, but they make the center-breaker failure the critical stability case, which deserves explicit study wherever a few circuits carry a large transfer. And at hot sites, cable connections for multi-kiloampere transformer circuits become impractical and GIL is the natural alternative.

16.3. Limitations

The studies are engineering models of the kind used in planning and specification, adequate to size equipment and expose design weaknesses. A project would repeat them with manufacturer and utility data: frequency-dependent line models and measured arrester characteristics in the EMT studies, detailed generator, excitation and STATCOM models in the stability study (which would lengthen the CCTs), detailed GIS geometry for the VFTO study, a harmonic survey for the MSCDN damping design, a Wenner survey interpreted with the same two-layer model for the grid, and project-specific prices for the economic comparisons. The network equivalents are representative rather than taken from a specific utility.

17. Conclusion

An 1100-kV ac grid substation delivering 10 GW into a 400-kV network has been designed and verified by simulation from a single consistent data set. Four 1100-kV feeders in two corridors and twelve 420-kV feeders on six routes deliver the load with all voltages and loadings within limits under all 22 single contingencies, with voltage-stability margins of 55% intact, 38% with one 320-km feeder out and 21% with a whole corridor out. Five 3 × 1000-MVA autotransformer banks give a transformation capacity that is firm electrically (91.9% worst N-1 loading with automatic bus-section reconfiguration) and thermally (105.7 °C hot spot on a 50 °C day).

The verification changed the design in six places: a 10-Ω neutral reactor that reduces the 420-kV single-phase fault from the full 63-kA rating to 48.4 kA, below the three-phase level; 1600 Mvar of 420-kV switched capacitors that keep the STATCOMs in reserve; 1.1-GW generation rejection on center-breaker failure, which raises the CCT from 108 to 166 ms; transformer-terminal and bay-located gas-insulated arresters, with 400-Ω closing resistors and 500-Ω disconnector damping resistors, giving margins of 3.7–8.5% and 15.5% on the 1800-kV and 2400-kV withstand levels; 420-kV GIL for the transformer connections; and a grounding design based on the 69.8-kA reversed-neutral grid current, with a ground potential rise of 5.42 kV and a worst touch voltage of 283 V against 998 V permissible. The substation operates at 99.83% efficiency at full load. Because these findings stem from the properties of autotransformers, one-and-a-half-breaker diameters, GIS–GIL paths and hot-site thermal conditions, a simulation-based verification of this kind is recommended for any UHV substation design.

References

1. Liu, Z. (2014). Ultra-high voltage AC/DC grids. Academic Press.
2. Shu, Y., & Chen, W. (2018). Research and application of UHV power transmission in China. High voltage, 3(1), 1-13.
3. CIGRE, W. (2008). A3. 22: Technical Requirements for substation equipment exceeding 800 kV. CIGRE TB, 362.
4. CIGRE, W. (2011). A3. 22: Background of technical specifications for UHV substation equipment. CIGRE Technical Brochure, 462.
5. CIGRE WG A3.28, "Switching phenomena for EHV and UHV equipment," CIGRE, Paris, France, Tech. Brochure 570, 2014.
6. UHV AC Transmission Systems, IEC TS 63042 series (Parts 101, 201, 301 and 302), IEC, Geneva, Switzerland.
7. R. Hileman (1999), Insulation Coordination for Power Systems. New York, NY, USA: Marcel Dekker.
8. Insulation Co-Ordination—Part 4: Computational Guide to Insulation Co-Ordination and Modelling of Electrical Networks, IEC TR 60071-4:2004.
9. Martinez-Velasco, J. A. (2010). Power System Transients: Parameter Determination. IEEE Power and Energy Magazine, 8(6), 104.
10. Koch, H. (2012). Gas insulated transmission lines (GIL). West Sussex.
11. Koch, H., Benato, R., Laußegger, M., Köhler, M., Leung, K. K., Mirebeau, P., ... & Bowmann, G. (2008). Application of long high capacity gas-insulated lines in structures. ELECTRA, 3(240), 29-37.
12. Kimbark, E. W. (1964). Suppression of ground-fault arcs on single-pole-switched EHV lines by shunt reactors. IEEE Transactions on Power Apparatus and Systems, 83(3), 285-290.
13. Dawalibi, F., & Mukhedkar, D. (1975). Optimum design of substation grounding in a two layer earth structure: Part I□Analytical study. IEEE Transactions on Power Apparatus and Systems, 94(2), 252-261.
14. Heppe, A. J. (1979). Computation of potential at surface above an energized grid or other electrode, allowing for non-uniform current distribution. IEEE Transactions on Power Apparatus and Systems, (6), 1978-1989.
15. Sverak, J. G. (1984). Simplified Analysis of Electrical Gradients Above a Ground Grid, Part I: How Good Is the Present IEEE Method? (A Special Report for WG78. 1). IEEE Power Engineering Review, (1), 26-27.
16. IEC Standard Voltages, IEC 60038:2009.
17. Transformers—Part, P. (2011). 2: Temperature Rise for Liquid-Immersed Transformers. Standard IEC, 60, 076-2.
18. Carson, J. R. (1926). Wave propagation in overhead wires with ground return. The Bell System Technical Journal,

5(4), 539-554.
19. Deri, A., Tevan, G., Semlyen, A., & Castanheira, A. (1981). The complex ground return plane a simplified model for homogeneous and multi-layer earth return. IEEE Trans Power App Syst, (8), 3686-3693.
20. IEEE Standard for Calculating the Current-Temperature Relationship of Bare Overhead Conductors, IEEE Std 738-2012.
21. CIGRE WG B2.43, "Guide for thermal rating calculations of overhead lines," CIGRE, Paris, France, Tech. Brochure 601, 2014.
22. Peek, F. W. (1929). Dielectric phenomena in high-voltage engineering. McGraw-Hill Book Company, Incorporated.
23. Anderson, P. M. (1995). Analysis of faulted power systems (Vol. 11). John Wiley & Sons.
24. Tinney, W. F., & Hart, C. E. (1967). Power flow solution by Newton's method. IEEE Transactions on Power Apparatus and systems, (11), 1449-1460.
25. Short-Circuit Currents in Three-Phase A.C. Systems—Part 0: Calculation of Currents, IEC 60909-0:2016.
26. Kundur, P., & Malik, O. P. (1994). Power system stability and control (Vol. 7, p. 623). New York: McGraw-hill.
27. Dommel, H. W. (1969). Digital computer solution of electromagnetic transients in single-and multiphase networks. IEEE transactions on power apparatus and systems, (4), 388-399.
28. H. W. Dommel, *EMTP Theory Book*, 2nd ed. Vancouver, BC, Canada: Microtran Power System Analysis Corp., 1992.
29. Insulation Co-Ordination—Part 2: Application Guidelines, IEC 60071-2:2018.
30. Power Transformers—Part 7: Loading Guide for Mineral-Oil-Immersed Power Transformers, IEC 60076-7:2018.
31. Swift, G., Molinski, T. S., & Lehn, W. (2001). A fundamental approach to transformer thermal modeling. I. Theory and equivalent circuit. IEEE transactions on Power Delivery, 16(2), 171-175.
32. Electric Cables—Calculation of the Current Rating—Part 1-1: Current Rating Equations (100% Load Factor) and Calculation of Losses—General, IEC 60287-1-1:2006+AMD1:2014; Part 2-1: Thermal Resistance, IEC 60287-2-1.
33. Anders, G. J. (1997). Rating of electric power cables: ampacity computations for transmission, distribution, and industrial applications.
34. Kuehn, T. H., & Goldstein, R. J. (1976). Correlating equations for natural convection heat transfer between horizontal circular cylinders. *Int J Heat Mass Transf, 19*(10), 1127-1134.
35. Churchill, S. W., & Chu, H. H. (1975). Correlating equations for laminar and turbulent free convection from a horizontal cylinder. International journal of heat and mass transfer, 18(9), 1049-1053.
36. Allan, R. N. (2013). Reliability evaluation of power systems. Springer Science & Business Media.
37. International Commission on Non-Ionizing Radiation Protection. (2010). Guidelines for limiting exposure to time-varying electric and magnetic fields (1 Hz to 100 kHz). Health physics, 99(6), 818-836.
38. High-Voltage Switchgear and Controlgear—Part 100: Alternating-Current Circuit-Breakers, IEC 62271-100:2021.
39. International Electrotechnical Commission. (2011). Short-Circuit Currents—Calculation of Effects—Part 1: Definitions and Calculation Methods.
40. HORIZONTALE, N. (2019). Insulation co-ordination–Part 1: Definitions, principles and rules.
41. Surge Arresters—Part 4: Metal-Oxide Surge Arresters Without Gaps for A.C. Systems, IEC 60099-4:2014; Part 5: Selection and Application Recommendations, IEC 60099-5:2018.
42. Boggs, S. A., Chu, F. Y., Fujimoto, N., Krenicky, A., Plessl, A., & Schlicht, D. (1982). Disconnect switch induced transients and trapped charge in gas-insulated substations. IEEE Transactions on Power Apparatus and Systems, (10), 3593-3602.
43. Ametani, A., Nagaoka, N., Baba, Y., Ohno, T., & Yamabuki, K. (2016). Power system transients: theory and applications. CRC Press.
44. Selection and Dimensioning of High-Voltage Insulators Intended for Use in Polluted Conditions—Parts 1 and 2, IEC TS 60815-1:2008 and IEC TS 60815-2:2008.
45. IEC 62067. (2011). Power cables with extruded insulation and their accessories for rated voltages above 150 kV (Um= 170 kV) up to 500 kV (Um= 550 kV) -test methods and requirements.
46. Swingler-UK, S., Daly-Ireland, J., Barber-Australia, K., Woschitz-Austria, R., Gille-Belgium, A., Antic-Croatia, J., ... & Aanhaanen-Netherlands, G. (2007). STATISTICS ON AC UNDERGROUND CABLE IN POWER NETWORKS.
47. IEC 62271-204. (2011). High-voltage switchgear and controlgear–Part 204: Rigid gas-insulated transmission lines for rated voltage above 52 kV.
48. Standard, I. E. C. (1989). Calculation of the cyclic and emergency current rating of cables-part 2: Cyclic rating of cables greater than 18/30 (36) kV and emergency ratings for cables of all voltages.
49. Shea, J. J., Hingorani, N. G., & Gyugyi, L. (2002). Understanding FACTS-concepts and technology of flexible AC transmission systems. IEEE Electrical Insulation Magazine, 18(1), 46-46.
50. International Electrotechnical Commission. (2014). Shunt Capacitors for AC Power Systems Having a Rated Voltage Above 1000V–Part 1: General.
51. Fakheri, E. A., Ware, B. J., & Shperling, B. R. (1978). Compensation scheme for single-pole switching on untransposed transmission lines. IEEE Transactions on Power Apparatus and Systems, (4), 1421-1429.
52. IEEE Guide for Safety in AC Substation Grounding, IEEE Std 80-2013.
53. EN50522, B. S. (2010). Earthing of power installations exceeding 1 kV ac. UK edition of Cenelec standard, (See page 1 col II para 1).
54. IEEE Substations Committee. (2012). IEEE guide for direct lightning stroke shielding of substations. IEEE, standard, 998.
55. Communication Networks and Systems for Power Utility Automation, IEC 61850 series.

56. Horowitz, S. H., Phadke, A. G., & Henville, C. F. (2022). Power system relaying. John Wiley & Sons.
57. IEEE Std. C37. 110-2007. (2007). IEEE Guide for the Application of Current Transformers Used for Protective Relaying Purposes.
58. CIGRE, W. (2009). B3. 20, "Evaluation of Different Switchgear Technologies (AIS, MTS, GIS) for Rated Voltages of 52 kV and Above,". ELECTRA, (245).

Appendix: Model Data

All per-unit values are on 1000 MVA and base voltages of 1000, 400 and 63 kV (Tables 24 and 25).

Branch	Length	R (p.u.)	X (p.u.)	B/2 (p.u.)
L1, L2: A–U	280 km	0.00218	0.07013	0.6335
L3, L4: B–U	320 km	0.00246	0.07978	0.7257
R1: S4, S2–LC1	60 km	0.00655	0.09472	0.02176
R2: S2, S1–LC2	80 km	0.00872	0.12623	0.02902
R3: S1, S3–LC3	100 km	0.01089	0.15768	0.03629
R4: S1, S4–LC4	70 km	0.00764	0.11048	0.02539
R5: S1, S3–LC5	90 km	0.00981	0.14196	0.03266
R6: S1, S3–LC6	120 km	0.01304	0.18906	0.04357
EXT–LC2, EXT–LC5 (×2 each)	60 km	0.00655	0.09472	0.02176

Table 24: Branch Data (Positive Sequence, Exact II)

Element	Data
Bank (each)	z_H = 0.0001 + j0.1541, z_M = 0.0001 − j0.0880, z_T = 0.0004 + j0.5281; taps ±8 × 1.25%
Neutral reactor	10 Ω (0.0625 p.u. on 400 kV), n = 2.5
Line reactors	960 Mvar at U, 240 Mvar remote, at 1050 kV
Hub A (slack)	7300 MVA; X″ 0.25, X′ 0.35, H 4.5 s; 1.05 p.u.; local load 600 MW
Hub B	6700 MVA; X″ 0.25, X′ 0.35, H 4.5 s; 5500 MW; 1.05 p.u.; local load 500 MW
Regional grid EXT	5500 MVA; X″ 0.25, X′ 0.35, H 27.3 s; 5000 MW; load 5000 MW
Load centers LC1–LC6	1800/1700/1600/1700/1600/1500 MW at 0.95 p.f.
Regional ties	LC1–2–3–4–5–6–1: 45/50/55/50/45/65 km of 400-kV line
Zero sequence	Sources X_0/X_1 = 0.7; ultimate infeed z = 0.0161 p.u., X/R 32

Table 25: Transformer, Reactive-Plant and Source Data

The arrester switching characteristic used in the EMT models is 1430 kV at 1 kA, 1460 kV at 2 kA, 1570 kV at 10 kA and 1620 kV at 20 kA; the EMT time steps are 10 μs (energization) and 2 ns (lightning).

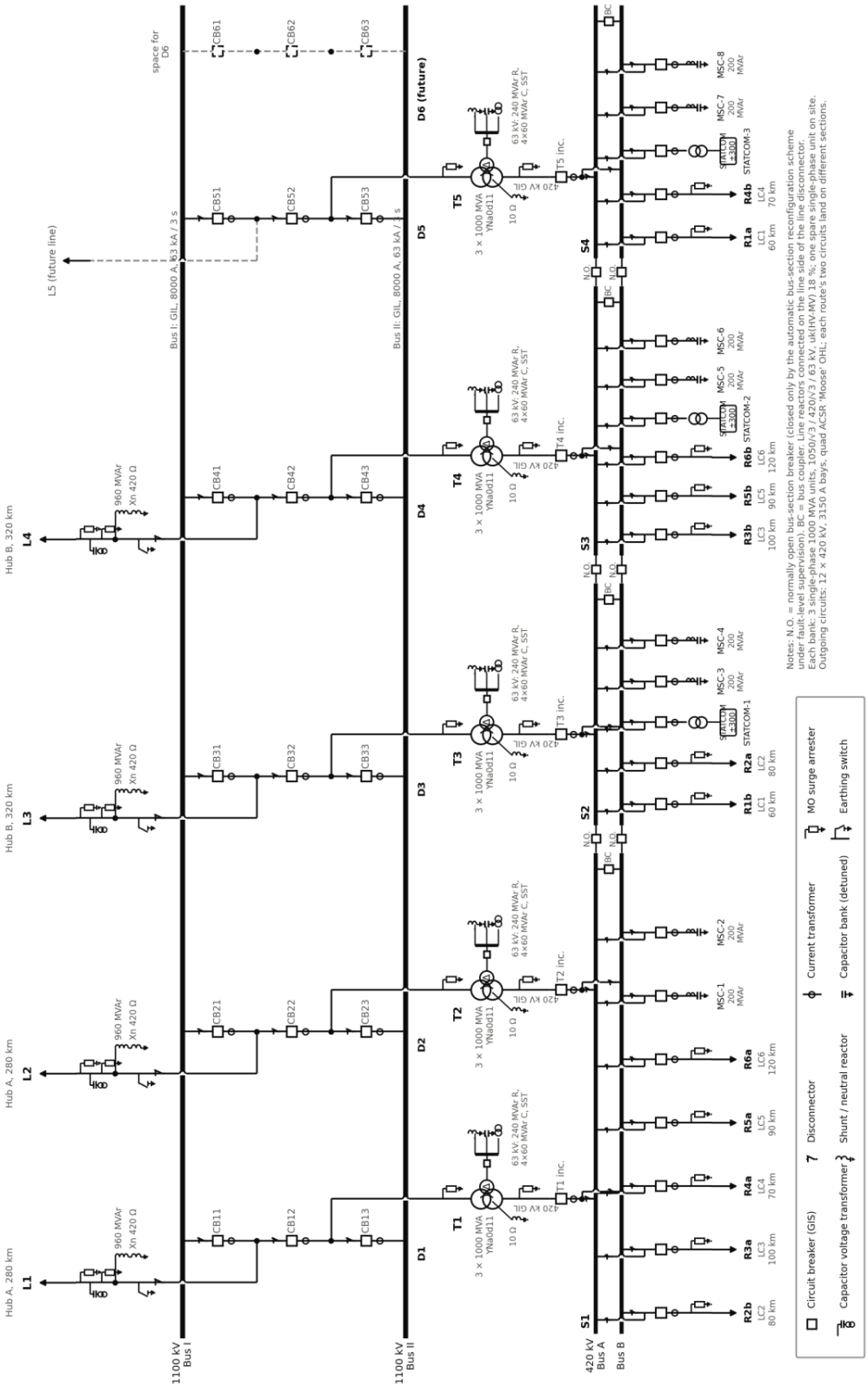
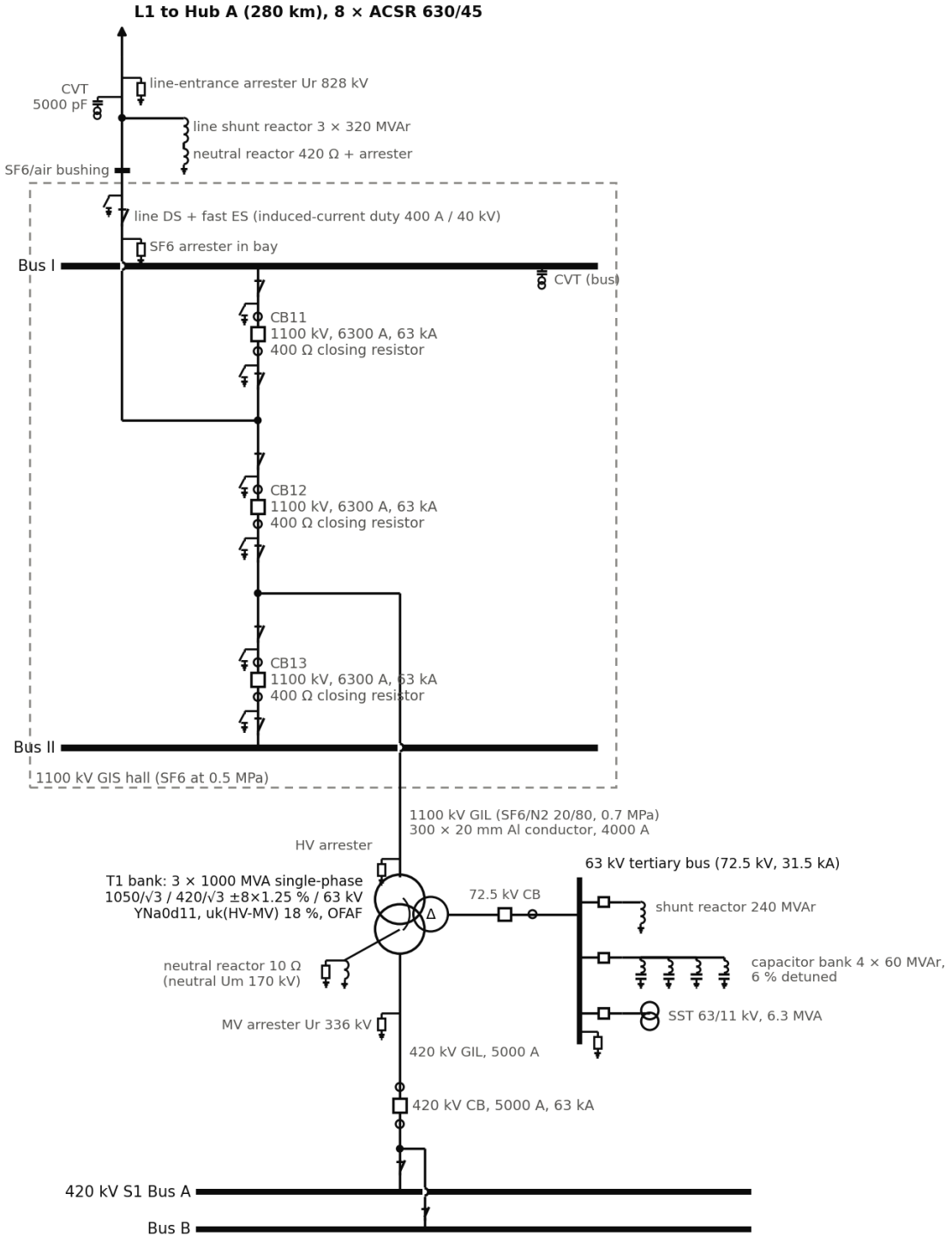


Figure 7: Overall Single-Line Diagram of the Substation: Four Incoming 1100-kV Feeders (L1–L4) with 960-Mvar Line Reactors, the 1100-kV One-and-a-Half-Breaker GIS with Five Equipped Diameters, Five 3 × 1000-MVA Autotransformer Banks With 10-Ω Neutral Reactors and Tertiary Plant, the Four-Section 420-kV Double-Busbar GIS, and Twelve Outgoing 420-kV Feeders (R1a–R6b) with Eight 200-Mvar MSCs and three ±300-Mvar STATCOMs.



Symbols to BS EN 60617. Each circuit breaker has current transformers on both sides so that adjacent protection zones overlap.

Figure 8: Single-Line Diagram of Diameter D1: Line Entrance with Line-Entrance Arrester, CVT and 960-Mvar Reactor with 420-Ω Neutral Reactor; GIS Diameter with 400-Ω Closing Resistors; 1100-kV GIL to Bank T1; 63-kV Tertiary with 240-Mvar Reactor, 4 × 60-Mvar Detuned Capacitors and Station-Service Transformer; 420-kV GIL and Incomer to Section S1.